Volume 1 | Number 1 | Jan 2013 | Pages 1–100

Catalysis
Science &
Technology

www.rsc.org/catalysis

ROYAL SOCIETY
OF CHEMISTRY

This is an *Accepted Manuscript*, which has been through the Royal Society of Chemistry peer review process and has been accepted for publication.

Accepted Manuscripts are published online shortly after acceptance, before technical editing, formatting and proof reading. Using this free service, authors can make their results available to the community, in citable form, before we publish the edited article. We will replace this *Accepted Manuscript* with the edited and formatted *Advance Article* as soon as it is available.

You can find more information about *Accepted Manuscripts* in the **Information for Authors**.

Please note that technical editing may introduce minor changes to the text and/or graphics, which may alter content. The journal's standard **Terms & Conditions** and the **Ethical guidelines** still apply. In no event shall the Royal Society of Chemistry be held responsible for any errors or omissions in this *Accepted Manuscript* or any consequences arising from the use of any information it contains.

www.rsc.org/catalysis

Catalysis Science & Technology

Paper

The interaction of reactants, intermediates and products with Cu ions in Cu-SSZ-13 NH$_3$ SCR catalysts: An energetic and ab initio X-ray absorption modeling study†
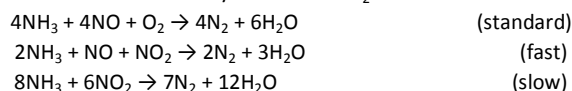
Renqin Zhang,[a] János Szanyi,[b] Feng Gao[b] and Jean-Sabin McEwen*[acd]

In this contribution, the most likely positions for Cu in Cu-SSZ-13 with a single charge compensating Al atom (ZCu) at a Si:Al ratio of 11:1 was investigated, including the effect of the adsorption of reactants, intermediates, and products that one would find in a NH$_3$ SCR reaction by using first-principles calculations based on density functional theory. The 6-membered ring (6MR) site is the most energetically favorable, while the 8-membered ring (8MR) sites are less favorable with energy differences about 0.5 eV with respect to the 6MR site for plain ZCu. Upon molecular adsorption, the energy differences between Cu in the 8MR and 6MR sites decrease and in some cases almost disappear. For the complex scenarios of NO or CO adsorption, the co-adsorption of 2 NO or 2 CO molecules, as well as NO or CO with OH and H$_2$O, weakens the interaction between adsorbates and Cu. The X-ray absorption near edge structure (XANES) of Cu in Cu-SSZ-13 under different conditions was also modeled from first principles. A small peak feature around 8979.5 eV was found in the K-edge XANES of Cu for a clean ZCu conformation with Cu in an 8MR site while this feature is absent when Cu is in a 6MR site. We correlate this result for this case as well as for other representative configurations by analyzing the corresponding PDOS of the excited state of Cu while taking into account the core-hole effect. Molecular adsorption onto Cu in a 6MR or an 8MR site results in a Cu K-edge XANES that is independent on its location. When NO (or CO, N$_2$) is adsorbed onto Cu in ZCu, a small peak feature in the K-edge XANES appears at 8.98 keV, which is induced by the splitting of the Cu 4p state. An analysis of the XANES in the presence of two co-adsorbed species on an isolated Cu ion shows that the K-edge position of Cu has the following order (from low to high energy): clean < M < M+H$_2$O < 2M < M+OH (M denotes NO or CO). As a result, we conclude: (1) XANES can readily distinguish between adsorbates on ZCu due to their different oxidizing capacities; but (2) XANES cannot be used to distinguish between the Cu location/oxidation state in the presence of adsorbates, except in the presence of H$_2$O and NH$_3$ where such distinctions can be made.

Introduction

Nitrogen oxides (NO$_x$) are one of the main air pollutants and they are present in the exhaust from diesel engines, which are popular in road transport due to their efficiency and durability.[1] However, NO$_x$ emission control is a challenge in "lean-burn" engines.[2] As is well known, the selective catalytic reduction (SCR) of NO$_x$ with ammonia is a reaction between the NO, NO$_2$, and O$_2$ oxidants and the NH$_3$ reductant to form N$_2$ and H$_2$O. The application of NH$_3$ as a reductant in NO$_x$ SCR provides an improved solution to lean NO$_x$

a. *The Gene and Linda Voiland School of Chemical Engineering and Bioengineering, Washington State University, Pullman, WA 99164.E-mail: js.mcewen@wsu.edu*
b. *Institute for Integrated Catalysis, Pacific Northwest National Laboratory, Richland, WA 99352.*
c. *Department of Physics and Astronomy, Washington State University, Pullman, WA 99164.*
d. *Department of Chemistry, Washington State University, Pullman, WA 99164*
† Electronic Supplementary Information (ESI) available: Plots of energy as a function of volume; local structures; energy differences and bond lengths; effect of unit cell and functionals on Cu K-edge XANES; comparison between computational and experimental Cu K-edge XANES; XANES and corresponding PDOS for N$_2$_ZCu; XANES for HONO, N$_2$O, NO$_2$, NO$_3^-$, O$_2$, and OH$^-$ adsorbed within ZCu; as well as the structure of a hydrated Cu-SSZ-13 model catalyst. See DOI: 10.1039/x0xx00000x

after treatment over the traditional three-way catalysts. Three general types of NH$_3$ SCR chemistries are generally distinguished based on the stoichiometry of NO and NO$_2$:

$$4NH_3 + 4NO + O_2 \rightarrow 4N_2 + 6H_2O \quad \text{(standard)}$$
$$2NH_3 + NO + NO_2 \rightarrow 2N_2 + 3H_2O \quad \text{(fast)}$$
$$8NH_3 + 6NO_2 \rightarrow 7N_2 + 12H_2O \quad \text{(slow)}$$

Copper-exchanged SSZ-13 (Cu-SSZ-13), a zeolite with the chabazite (CHA) structure, was reported to be more active and selective toward the formation of N$_2$ in the reduction of NO with NH$_3$ as compared to Cu-ZSM-5 and Cu-beta.[3] Also, it was found that Cu-SSZ-13 is more hydrothermally stable than the Cu-Y, Cu-ZSM-5, and Cu-beta zeolites.[4] The enhanced stability of Cu-SSZ-13 is rationalized in terms of the small pore structure (3.8 Å, diameter of 8-member ring channel) of this zeolite catalyst. Additionally, XRD patterns show that the thermal stability of SSZ-13 is increased significantly when copper is exchanged into the extra-framework as compared with the acid form of the zeolite.[5] Using H$_2$-TPR, Kwak, *et al.* found that below ~600 °C, Cu^{2+} could be reduced to Cu$^+$ and to Cu^0 in Cu-ZSM-5 and Cu-beta, while Cu^{2+} could only be reduced to Cu$^+$ in Cu-SSZ-13.[4] The Cu$^+$/Cu^{2+} redox cycle was found to play a significant role in SCR catalysis.[6-9] Furthermore, it was reported that the SCR reaction could be divided into two half-reactions: an

oxidation of the catalyst by $NO+O_2$ and a reduction by $NO+NH_3$.[10, 14] Therefore, it is probable that the barriers for the two half-reactions are correlated to the SCR efficiency of Cu-SSZ-13.

X-ray absorption spectroscopy (XAS) is a versatile tool to determine the oxidation state and the local structure of Cu in Cu-exchanged zeolites. In recent years, XANES has been widely used to study the properties of Cu-SSZ-13 because of its high activity and selectivity in the NH_3 SCR of NO_x. In an *operando* XAS study, Kispersky *et al.* proposed that the SCR reaction occurs on Cu-exchanged zeolites (SSZ-13 and ZSM-5) via a redox mechanism between the Cu^{2+} and Cu^+ oxidation states.[7] The same conclusion was also made by Ribeiro and co-workers in an integrated experimental and theoretical study of the NH_3-SCR of NO_x in SSZ-13.[6] Under fast and slow SCR conditions, in which NO_2 is half or all of the NO_x feed, respectively, Cu^{2+} remains as the only evident Cu oxidation state. Under more reducing standard SCR conditions, where there is no NO_2 in the feed, a Cu^+ species also appears.[6] Combining XAS with other experimental techniques, Peden and co-workers[11,12] and Yang *et al.*[13] proposed that a key step in SCR is that Cu^{2+} is reduced to Cu^+ by NO, leading to the formation of the spectroscopically observed Cu-nitrosyl complex. A detailed discussion of this proposed mechanism can be found in the recent paper reported by Gao, *et al.*[12] More recently, a XAS study by Beato and co-workers concluded that the bidentate nitrate species (i.e., Cu^{2+}-NO_3^-) is formed upon exposure of Cu^+ to a mixture of NO and O_2 or to NO_2 and the formation of Cu^{2+}-NO_3^- is rate-determining for the standard SCR reaction.[10] On the other hand, Paolucci *et al.* demonstrated that NO and NH_3 together are necessary for Cu^{2+} reduction to Cu^+ and both NO and O_2 are necessary for the oxidation of Cu^+ to Cu^{2+} through a XANES analysis of their reactant cutoff experiments.[14]

Despite the advances, the nature of the active site is still very much a debated topic. In some reported results the Cu K-edge XANES were used to identify the active Cu site in reactions on Cu-SSZ-13.[6, 15-17] Combined with other experimental tools (such as infrared spectroscopy), XANES is also used to follow the movement of Cu ions in SSZ-13 under different conditions of dehydration, reduction, and molecular adsorption.[18] These results aid the identification of the location, coordination, and oxidation states of Cu in Cu-SSZ-13. For example, by combining XAS experiments under *operando* conditions with a calculation of the phase diagram from first principles, the local environments of the exchanged Cu^+ and Cu^{2+} ions under different gas conditions were assigned.[6] Under "fast" SCR conditions, the XANES features were assigned to two types of Cu^{2+} ion environments, both with a coordination number of 4. Under "standard" SCR conditions, the appearance of a new signal assigned to the Cu^+ ion with adsorbed H_2O and reduction in the average Cu coordination were established. However, the analysis of the experimental Cu K-edge XANES results relies heavily on the comparison with proper reference species. Moreover, as reported by Kispersky *et al*,[7] *in situ* (instead of *in operando*) XAS may lead to inaccurate "counting" of active Cu-ions.

Some other issues that still need to be addressed for CHA-based SCR catalysts include the effect of reactants on the Cu location and the reaction mechanism itself. Experimental evidence has demonstrated that Cu ions are the active sites for NH_3-SCR reactions.[15, 19, 20] However, the location of the Cu ions in the Cu-SSZ-13 zeolite, especially under reaction conditions, is still unclear. It is reported that higher Cu loadings can also result in multiple Cu locations within the zeolite framework.[20, 21] Note that the 8-membered ring has two sides available to interact with adsorbates while the 6-membered ring has only one available side. It also appears that Cu species are mobile under reaction conditions.[9,18, 21, 22]

In addition to examining the effects of NH_3 SCR reactants on Cu-SSZ-13, we will also investigate the adsorption of CO. Although CO is not a SCR ingredient; it is an important emission from gasoline-powered vehicles.[23] CO can also be used to probe the properties (e.g., location and local environments) of Cu^+ ions.[24] Further, significant variation in the near-edge structure of the Cu K-edge XANES for a Cu-exchanged Y zeolite were reported in the presence of CO.[25] Subsequently, it was found that CO interacts with Cu ion by modifying the coordination environment of the metal ion.[25] Here we will closely compare our modeling results to the recent XANES study of Kwak et al. in order to shed light on such experimental results.[18]

As part of our continuing efforts toward understanding the catalytic properties of Cu-SSZ-13, this contribution has two parts. In the first part, a first principles study of the adsorption of typical NO_x SCR reactants, possible intermediates, and products on an isolated Cu ion were performed. The Cu ion is anchored within one of the 6-membered or one of the 8-membered rings that make up the SSZ-13 framework. In the second part, the Cu K-edge XANES of Cu-SSZ-13 under different conditions were calculated using first principles. This will serve as an alternative way to analyze the experimental XAS under SCR reaction conditions without making use of experimental reference samples.[26] A comparison between the computational XANES results and the available experimental XANES results will be discussed.

Computational details

The DFT calculations for the energetics were performed with the Vienna *Ab initio* Simulation Package (VASP).[27, 28] The projector augmented-wave (PAW)[29, 30] method and the generalized-gradient approximation (GGA), using the PW91 functional,[31] were employed for the treatment of the electron-ion interactions and the exchange-correlation effects, respectively. With its PAW potentials, VASP combines the accuracy of all-electron methods with the computational efficiency of plane-wave approaches. The total energy convergence threshold was set to 10^{-8} eV and the geometries were considered to be fully relaxed when the forces were less than 0.01 eV/Å. A 400 eV plane-wave cut-off and a single Γ-point sampling of the Brillouin zone were used for the optimization calculations. To test the accuracy of our calculations, we preformed calculations with a high cut-off energy of 500 eV. Using NO adsorption as an example, an adsorption energy of 1.268 eV is obtained at this cut-off energy. With a lower cut-off energy of 400 eV, the calculated adsorption energy is 1.271 eV. The difference

2 | *Catal. Sci. Technol.*, 2015, **00**, 1-15

This journal is © The Royal Society of Chemistry 20xx

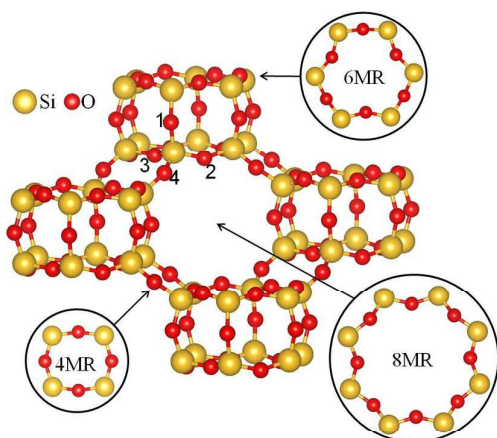Catalysis Science & Technology Accepted Manuscript

Fig. 1 Structure of pure SSZ-13. There are four nonequivalent O sites, which are labeled by numbers 1-4. Locations of 4MR, 6MR and 8MR are also displayed. Large and small spheres represent Si and O atoms, respectively.

between them is 0.003 eV. Therefore we believe that the accuracy of our calculations is good within the GGA. As such, for the calculations of adsorption energy, an upper limit of 0.01 eV in error is given when the calculations are within the GGA.

As is well known, the SSZ-13 zeolite belongs to the CHA structure, which is composed of 4-membered rings (4MR), 6-membered rings (6MR), and 8-membered rings (8MR). There are two equivalent ways to construct the chabazite unit cell. One is the hexagonal cell with 36 symmetry-equivalent tetrahedral (T) sites and 72 O atoms. The other one is a rhombohedral cell, which contains 12 T sites and 24 O atoms. All T sites are crystallographically equivalent and there are four nonequivalent O sites, which can be distinguished according to their participation in different rings of the framework. As shown in Fig. 1, the oxygen O1 belongs to two 4MRs and one 8MR; O2 belongs to one 4MR, one 6MR, and one 8MR; O3 belongs to two 4MRs and one 6MR; and finally O4 participates in one 4MR and two 8MRs. As reported by McEwen, et al.,[6] the local coordination of Cu with O gives the same results when a unit cell with a Si:Al ratio of 11:1 or 35:1 is used. Hence, we will limit ourselves to a Si:Al ratio of 11:1, for which the rhombohedral unit cell is the most convenient.

In order to obtain an accurate equilibrium volume, a three-step procedure was performed, as detailed in the Supporting Information. For the purely siliceous chabazite, this procedure gives an equilibrium rhombohedral volume of 813.1 $Å^3$, which is consistent with previous calculations (see Fig. S1).[6, 32, 33] In a rhombohedral unit cell, one Si atom can be replaced by one Al atom, which results in a one electron-deficit because the number of valence electrons in Si and Al are 4 and 3, respectively. A Cu^+ ion can then be used to compensate for this electron-deficit. The Cu^+ ion can be oxidized further through interactions with other adsorbates resulting in a change in its oxidation state. This unit cell is presented as ZCu, where there is one Al atom in the rhombohedral framework and the negative framework charge is compensated by a Cu^+ ion. The calculated equilibrium volume of ZCu is 823.6 $Å^3$, which is larger than the SSZ-13 zeolite and is also

consistent with the result reported by McEwen, et al.[6] The Cu binding energy is calculated by

$$E_b = E_{ZCu} - E_{SSZ-13} - E_{bulk}^{Cu} \qquad (1)$$

where E_{ZCu}, E_{SSZ-13}, and E_{bulk}^{Cu} are the total energies of ZCu, ZCu without Cu, and bulk Cu, respectively.

For the molecular adsorption calculations, the unit cell with NO adsorbed in the ZCu conformation was found to not change the equilibrium volume. Other adsorbates were studied in the unit cell using the lattice constants identified for NO adsorbed on ZCu. Adsorption energies, E_{ads}, were calculated by using the following equation:

$$E_{ads} = E_{tot} - E_{ZCu} - E_{mol} \qquad (2)$$

where E_{tot}, E_{ZCu}, and E_{mol} are the total energies of ZCu in the presence of molecular adspecies, clean ZCu, and the isolated molecules in gas phase, respectively. For the 2M_ZCu, M+OH_ZCu and M+H$_2$O_ZCu co-adsorption systems (where M represents either a NO or a CO molecule), the adsorption energies of NO (or CO) are defined as:

$$E_{ads}^M = (E_{tot} - E_{ZCu}^{withoutM} - NE_M)/N \qquad (3)$$

where E_{tot}, $E_{ZCu}^{withoutM}$, and E_M are the total energies of ZCu with co-adsorbed molecular species, a ZCu catalyst in absence of NO and CO, and isolated NO (or CO) molecules in the gas phase, respectively. N is the number of adsorbed NO (or CO) molecule(s) in the system. Note that a $[Cu^{2+}(OH^-)]^+$ product is formed when a neutral OH reactant adsorbs on an isolated Cu^+ ion in our calculations, where an electron is transferred from the Cu^+ ion to the OH species.

Unless indicated otherwise, the calculations of the theoretical K-edge XANES and the corresponding projected density of states (PDOS) analyses of Cu in Cu-SSZ-13 were performed using the CASTEP code.[34] Note that the core-level spectra are studied through the electron energy loss spectra calculations (EELS) within CASTEP.[26] EELS and XANES are identical in principle. In order to avoid confusion, EELS is referred to as theoretical XANES in this contribution. CASTEP uses plane wave basis sets and ultrasoft pseudopotentials. The GGA-PBE[35] exchange-correlation functional was used for the structure optimizations and the XANES analyses in CASTEP. Note that the calculations of the XANES spectra were not affected whether or not one optimized the unit cell within CASTEP (see details in Fig. S2). As a result, the unit cell in CASTEP was not optimized; namely, the unit cell optimized by VASP was used to calculate the XANES.

Although the PBE, RPBE, or PBEsol functionals are recommended when performing the XANES calculations, the results of the theoretical K-edge XANES of Cu in ZCu with Cu in the 6MR site showed a weak dependence on the exchange-correlation functional (see Fig. S3). When the XANES calculations were performed, ultrasoft pseudopotentials were generated on the fly[26] where one core electron was removed from the 1s core level when performing core-hole calculations. It has been demonstrated that the core-hole effect has a significant influence on the core level spectra.[36] Therefore, the core-hole effect was accounted in our calculations. All core-hole calculations were carried out using supercells

sufficiently large so as to eliminate the interactions between periodic images. Previous work recommends a distance between the images of 8~10 Å.[26, 37] The dimensions of the rhombohedral unit cell used in our calculations satisfy this requirement. Energy cutoffs of 550 eV and a k-point grid of (5×5×5) were used in the calculations of the XANES. The energy broadening with an instrumental smearing, using the Gaussian method, of 0.6 eV and lifetime broadening of Cu with a value of 1.55 eV were applied.[26] The XANES intensity is proportional to the probability of absorption of a photon by a core electron.[38] It is reported that the calculated PDOS of O in final state, which includes the core-hole effect, correlates well with the corresponding O K-edge XANES of α-SiO$_2$.[39] The PDOS from the ground state calculation is quite different for the PDOS from the final state. Such a difference can be seen when examining Fig. S4 where we compare the PDOS of the Cu 4p in its ground state with the corresponding PDOS of the final state (excited state with a core-hole). As a result, we will be comparing the PDOS in the final (excited) state to our computed XANES spectra.

Results and Discussion

Positions of Cu in ZCu

The determination of the exact location of Cu cations in the zeolite framework and their local environment in the presence and absence of adsorbates is important for understanding the catalytic properties and the underlying SCR reaction mechanism. It has been reported that isolated Cu^{2+} ions are the active site in the SCR of NO$_x$ with NH$_3$ within the 6MR.[15, 19, 20] However, the influence of adsorbates on the Cu location and coordination has not been extensively investigated. Three possible positions of Cu in ZCu are considered in this contribution. One is located in the center of a 6MR and the other two are in the 8MR sites distinguished by bonding with different O atoms. Note that because of space restriction, the 4MR was found to be less favorable for Cu with respect to 6MR. In addition, when Cu is bound to a 4MR site, the adsorption of NO shifts it to the 6MR site during structure optimization. Therefore, 4MR sites were not investigated further in this contribution. As shown in Fig. 2, for the two positions of Cu in the 8MR sites, Cu atoms are bonded with O1 and O4 atoms or O2 and O4 atoms of the zeolite framework, which are labeled as 8MR_O14 and 8MR_O24 sites, respectively.

The Cu in the 6MR site was 3-fold coordinated with oxygen, where Cu is bonded to an activated O3 atom to form the smallest Cu-O bond length of 1.948 Å and two non-activated O3 atoms with longer Cu-O bond lengths of 2.004 and 2.363 Å, respectively. Here an activated O atom is denoted as one that is bonded to an adjacent Al atom and carries most of the negative charge due to the presence of Al^{3+} in the framework. An attempt was made to let Cu form bonds with two activated O atoms (O2 and O3), but the final structure reverted to that shown in Fig. 2 after optimization, where the Cu site forms bonds with one activated O atom and two non-activated O atoms. The Cu ions in both 8MR sites are 2-fold coordinated with two activated O atoms. In the 8MR_O14 site, the Cu-O bond lengths are 1.990 and 2.105 Å while they are 2.013 and
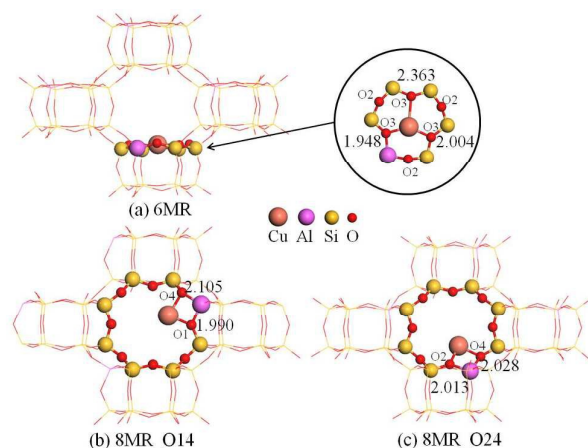

Fig. 2 Local structures of three possible Cu positions: (a) 6MR, (b) 8MR_O14, and (c) 8MR_O24 within the ZCu chabazite structure. Cu-O bond lengths with unit of Å are indicated in each panel. The legend of different atoms is displayed in the center. The different O atoms are labeled as presented in Fig. 1.

2.028 Å for Cu in the 8MR_O24 site. The average Cu-O bond lengths of Cu in 8MR_O14 and 8MR_O24 sites are 2.048 and 2.022 Å, respectively. As shown in Table 1, the coordination numbers of Cu in 6MR and 8MRs are 3 and 2, respectively.

Comparing the properties of Cu in different positions, the 6MR site was found to be thermodynamically the most favorable, as shown in Table 1. The 8MR_O14 and 8MR_O24 sites are slightly less favorable with total energy differences of 0.46 and 0.51 eV, respectively, as compared to the 6MR site. Based on the Cu binding energy results, Cu in the 6MR site has a stronger electrostatic interaction with the CHA framework and has a higher coordination with lattice oxygen atoms. The Cu binding energies are -1.41, -0.72, and -0.68 eV for Cu in the 6MR, 8MR_O14, and 8MR_O24 sites, respectively. It is concluded that for the ZCu conformation, the 6MR site is the most energetically favorable site while the 8MR sites are the second most favorable location for the Cu ions. These results are fully consistent with experimental discoveries[20, 21, 40] which found that there are two different types of Cu present in the SSZ-13 zeolite, namely, Cu ions primarily occupying sites in the 6MR at low Cu loading while at high Cu loading, some Cu ions are located in the large CHA cages and are close to the 8MR. In addition to this result, the integrated d-state electrons of Cu where found to be 9.7, 9.8, and 9.8 for Cu in the 6MR, 8MR_O14, and 8MR_O24 sites,

Table 1. Properties of possible Cu sites in ZCu. The energy difference is defined with respect to the total energy of the 6MR site. E_b was calculated by using Equation 1.

ZCu	6MR	8MR_O14	8MR_O24
Energy difference (eV)	0.00	0.46	0.51
Cu d-band center (eV)	-1.58	-1.70	-1.61
Average Cu-O bond length (Å)	2.105	2.048	2.022
Cu binding energy E_b (eV)	-1.41	-0.72	-0.68
Integrated electrons of d states	9.7	9.8	9.8
Coordination number (CN)	3	2	2

respectively, when performing a density of states analysis within the VASP code using the PW91 functional, confirming that the oxidation state of Cu in ZCu is Cu^+.

The concept of *d*-band center is one possible measure of the reactivity of transition metals.[41] The *d*-band center of Cu in the 6MR, 8MR_O14, and 8MR_O24 sites is -1.58, -1.70, and -1.61 eV, respectively, as shown in Table 1. There is a very slight difference between them, which suggests that the Cu ions in ZCu present similar catalytic properties independent of the location. Note that the 8MR sites are more accessible to reactants because of the increased space.

Molecular adsorption on ZCu

The adsorption properties of reactants, products, and possible intermediates on the active site are crucial to understanding catalyzed reactions. The adsorption of atomic or molecular species on the active site of the Cu-SSZ-13 modifies the electronic and structural properties of the system, thus affecting its catalytic properties. A detailed knowledge of the molecular adsorption properties of ZCu is necessary before undertaking a further study of its catalytic properties. Therefore, we studied the adsorption of the SCR reactants (NO, NO2, NH3, O2), products (N2, H2O, N2O) and possible intermediates (HONO, NO3-) on ZCu in this contribution. Note that a $[Cu2+(NO3-)]+$ product is formed when a neutral NO3 reactant adsorbs on an isolated $Cu+$ ion in our calculations, where an electron is transferred from the $Cu+$ ion to a neutral NO3 species. Although CO and CO2 molecules are neither reactants nor products in the SCR reactions, they are often used to study the properties of catalytically active sites and are always present in the exhaust gas stream under practical operating conditions. Therefore, the adsorption of CO and CO2 molecules on ZCu was also investigated. In addition, a humid environment is a more realistic picture of the practical application of the SCR zeolite, since engine exhausts contain large amounts of water, suggesting that there will be a large concentration of H2O surrounding the catalyst in the actual experiments. A few recent studies9,40 demonstrated that Cu-ions in the 8MR may form a $[Cu2+(OH-)]+$ complex, therefore the adsorption of OH on ZCu (labeled as OH_ZCu) was also studied. Knowing the molecular adsorption energies on Cu in different sites of ZCu is also of vital importance in understanding the catalytic properties of this catalyst. Table 2 lists the calculated adsorption

energies (according to Equation 2) of these molecules adsorbed on different Cu ions in ZCu.

As shown in Table 2, all molecules adsorbed on the Cu in 8MR sites presented stronger adsorption energies as compared to Cu in a 6MR site. The adsorption energy difference between molecules adsorbed on the Cu in the two 8MR sites is very small, where the largest difference of 0.18 eV occurs for the adsorption of the HONO intermediate and the smallest difference is only 0.03 eV for the adsorption of NH_3. Detailed information about structures of molecularly adsorbed species in a ZCu conformation can be found in Fig. S5. The following discussion provides more details about the behavior of molecular adsorption on ZCu. Note that the GGA functional has difficulty calculating the adsorption of NO and NO_2 and more accurate calculations can be obtained using a hybrid functional. It is concluded by Göltl et al. that in studying the adsorption of NO on Cu ions, adsorption energies calculated with hybrid functionals are lower and more realistic than those derived in the GGA.[33] However, this does not affect the energy differences given in Fig. 3, as was discussed in a previous paper.[22] Thus, since one of the main focuses of the present study is to obtain adsorption energy differences, our conclusions are not affected by restricting ourselves to the GGA. Nevertheless, the adsorption energies of NO and NO_2 on Cu using the HSE06 functional have been computed here and the results are shown in Table S1.

Among the reactants of NO, NH_3, NO_2, and O_2 in the NH_3 SCR reactions, the NH_3 molecule has the strongest adsorption energy. The O_2 molecule has the weakest binding to Cu, with an adsorption energy on Cu in the 6MR site being -0.64 eV, which is consistent with a value of -0.65 eV that can be found in literature.[6] As can be seen in Fig. S5, a side-on configuration, sometimes denoted as a $ZCu(\eta^2-O_2)$ conformation,[42] is the most favorable configuration when an O_2 molecule is adsorbed on Cu in a 6MR,[6] but an end-bound isomer is the most favorable configuration when an O_2 molecule is adsorbed on Cu in a 8MR. The adsorption energies of an O atom on the Cu ion in 6MR, 8MR_O14, and 8MR_O24 sites were also calculated. Note that the adsorption energy of an O atom was calculated with respect to the O_2 molecule. The positive adsorption energy of 0.51 eV means that it is energetically unfavorable to dissociate an O_2 molecule bonded to Cu in a 6MR. This conclusion is consistent with the result reported in the literature.[6]

The adsorption of NO_2 is more complicated. As studied using cluster models,[42] NO_2 presents several adsorption configurations on the Cu site. Five configurations of NO_2 adsorbed on ZCu with Cu in 6MR and 8MR sites were systematically investigated. The NO_2 adsorption energy values, as listed in Table 2, are also very similar to those reported on cluster models, where the adsorption energies were reported to vary from 1.03 to 1.48 eV depending on the underlying cluster model that was used.[42] Detailed structure and energetic information can be found in Fig.s S6-7 and Tables S2-3. A comparison of the most favorable configurations for NO_2 show that its adsorption configuration depends on whether the Cu ion lies in the 6MR or the 8 MR: a bidentate O-bound NO_2 is the most stable in the 8MR while a bidentate O and N side-bound NO_2 is the most stable in 6MR. The adsorption energies of the most favorable configurations for NO_2 are listed in Table 2. Note that the stronger binding of NO as compared to NO_2 is consistent with earlier cluster

Table 2. Molecular adsorption energies in a ZCu conformation with different Cu locations

Adsorbates	6MR	8MR_O14	8MR_O24
NO	-1.27	-1.78	-1.69
NO_2	-0.97	-1.44	-1.56
NH_3	-1.49	-2.02	-2.05
O_2	-0.64	-1.06	-1.14
N_2O	-0.79	-1.27	-1.36
HONO	-1.13	-1.52	-1.70
NO_3^-	-2.11	-2.49	-2.62
N_2	-0.81	-1.30	-1.39
H_2O	-0.89	-1.57	-1.70
OH^-	-2.61	-3.17	-3.23
CO	-1.60	-2.09	-1.99
CO_2	-0.11	-0.62	-0.69
$CO+OH^-$	-0.29	-0.44	-0.41

Catalysis Science & Technology

models, which also found a stronger binding of NO on Cu^+ as compared to NO_2 on Cu^+.

The main side product N_2O, along with the possible intermediates HONO and NO_3^- in NH_3 SCR, were found to have intermediate to strong interactions with ZCu. The N_2O molecule has relatively strong adsorption energies. The intermediate HONO has similar adsorption energies, as also displayed in Table 2. NO_3^- has the strongest interaction with Cu. Note that three NO_3^- configurations were investigated on a Cu site, namely, a monodentate nitrate with the N atom bound to Cu, a monodentate nitrate with the O atom bound to Cu and a bidentate nitrate with two O atoms bound to Cu. Only the bidentate configuration of two O atoms bound to Cu is stable, as shown in Fig. S5. This configuration is consistent with the proposed structure of $Cu-NO_3^-$ in the recent work of Beato and coworkers.[10]

For OH_ZCu, OH interacts very strongly with Cu ion because of its strong oxidizing power. The change in oxidation state of Cu with OH adsorption was verified by integrating the d-state electrons of Cu within the VASP code. The integrated d-state electrons of Cu in the 8MR_O14 site was 9.2, which means that Cu is oxidized by OH from Cu^+ to Cu^{2+}. This implies that the formation of the $[Cu^{2+}(OH^-)]^+$ species occurs in this situation and confirms the reported conclusion that not all of the Cu^{2+} ions initially present in the zeolite are balanced by two Al atoms.[40] Some Cu^{2+} ions can certainly stay in the form of a nominal monovalent $[Cu^{2+}(OH^-)]^+$ species,[9, 40, 43] which balances the negative charge created by one Al atom within the zeolite. It is reported that the Cu^+/Cu^{2+} redox reaction occurs during the NH_3-SCR reaction.[7-9, 12] The OH group may play an important role in the Cu^+/Cu^{2+} redox reaction due to its oxidation of a Cu^+ ion to a Cu^{2+} ion. In addition, the adsorption of OH stabilizes the Cu ion within the 8MR site making this site more favorable as compared to the 6MR. This result supports the proposed location of Cu next to the 8MR by Gao $et\ al.$[9]

Out of the spectator species CO and CO_2, the adsorption energies of CO on the $[Cu^{2+}(OH^-)]^+$ species are -0.29, -0.44, and -0.41 eV for the 6MR, 8MR_O14, and 8MR_O24 sites, respectively, as shown in Table 2. These results demonstrate that CO interacts weakly with Cu^{2+}. In the presence of both Cu^{2+} and Cu^+, CO interacts selectively with Cu^+ ions. As such, CO can be used to probe the properties (e.g., location and local environments) of Cu^+ ions.[12] As shown in Table 2, CO strongly adsorbs on the Cu^+ sites in a ZCu conformation. However, the adsorption of CO_2 on the ZCu sites is much weaker.

In order to understand the thermodynamic stability of ZCu with adsorbates, the adsorption energy differences and the total energy differences between Cu in the different Cu sites (6MR, 8MR_O14, 8MR_O24) were compared. The total energy differences between Cu in the 8MR and the 6MR, ΔE_1 and ΔE_2, are defined as follows:

$$\Delta E_1 = E_{8MR\_O14} - E_{6MR} \ \text{ and } \ \Delta E_2 = E_{8MR\_O24} - E_{6MR} \qquad (4)$$

where E_{6MR}, E_{8MR_O14}, and E_{8MR_O24} are the total energies of the ZCu conformation in the presence of one of the species given in Table 2 adsorbed on a Cu ion that is located in a 6MR, a 8MR_O14, and a 8MR_O24 position, respectively. We compare these results to ΔE_1^{clean} and ΔE_2^{clean}, the corresponding energy differences between the 8MR and 6MR in the absence of adsorbates. On the other hand,
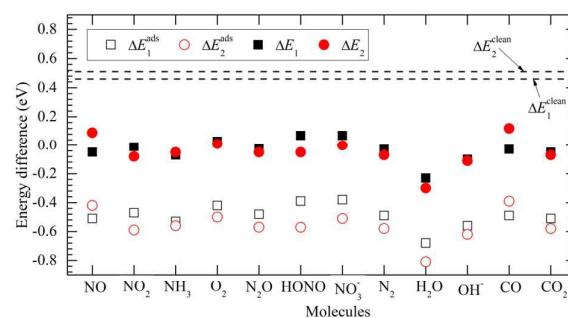

Fig. 3 The adsorption energy differences, ΔE^{ads} (unfilled symbols), and total energy differences, ΔE (solid-filled symbols), of Cu in the 6MR and 8MR positions. The subscripts 1 and 2 correspond to the 8MR_O14 site and 8MR_24 site, respectively. The total energy differences of the clean ZCu conformations with Cu in the 6MR and 8MR sites, ΔE_1^{clean} and ΔE_2^{clean}, are calculated to be 0.46 eV and 0.51 eV, respectively, which are shown as dashed lines. Note that the energy differences with respect to the 8MR_O14 and 8MR_O24 sites are small.

the adsorption energy differences, ΔE^{ads}, for Cu located in one of the 8MR sites and the 6MR site are defined as:

$$\Delta E_1^{ads} = E_{8MR\_O14}^{ads} - E_{6MR}^{ads} \ \text{ and } \ \Delta E_2^{ads} = E_{8MR\_O24}^{ads} - E_{6MR}^{ads} \qquad (5)$$

where E_{6MR}^{ads}, $E_{8MR\_O14}^{ads}$, and $E_{8MR\_O24}^{ads}$ are the adsorption energies (as given by Equation 2) of one of the species given in Table 2 adsorbed on a Cu ion that is located in a 6MR, a 8MR_O14, and a 8MR_O24 position, respectively.

As shown in Fig. 3, the total energy differences, ΔE_1 and ΔE_2, of molecularly adsorbed ZCu are smaller than that of clean ZCu, $i.e.$ ΔE_1^{clean} and ΔE_2^{clean}. This implies that the adsorption of reactants, intermediates, products, and spectators decrease their energy differences between Cu in the 8MR and 6MR sites of ZCu. For example, ΔE_1 and ΔE_2 for NO adsorption on ZCu are -0.05 and 0.09 eV, which decreased by 0.51 and 0.42 eV with respect to clean the ZCu conformations. Also, ΔE_1 and ΔE_2 distribute evenly around an energy difference of 0 eV, except for H_2O adsorbed ZCu. This means that the thermodynamic stability of molecularly adsorbed ZCu is almost the same for each of the different Cu sites. When considering the adsorption of H_2O, ΔE_1 and ΔE_2 are -0.23 and -0.30 eV, respectively, which are the largest energy differences among all adsorbates studied here. These values suggest that the most favorable position of Cu shifts from the 6MR for clean ZCu to the 8MR sites for ZCu with H_2O adsorption. The adsorption of H_2O on ZCu also gives the largest adsorption energy differences, as shown in Fig. 3, which are -0.69 and -0.81 eV for Cu in the 8MR_O14 and 8MR_O24 sites, respectively. Further discussion regarding the adsorption of H_2O on ZCu will be provided later in this contribution. As mentioned above (Table 2), stronger adsorption energies are realized for adsorption on Cu-ions in 8MR as compared to their counterparts located in 6MR. As shown in Fig. 3, the distribution of ΔE_1^{ads} and ΔE_2^{ads}, as defined by Equation 4, cancels to a large extent the adsorption preference in the 6MR of a bare Cu species (ΔE_1^{clean} and ΔE_2^{clean}), except for the adsorption of H_2O. As a result, ΔE_1 and ΔE_2, the total energy differences between the 8MR and 6MR configurations as defined in Equation 5, are close to zero in the
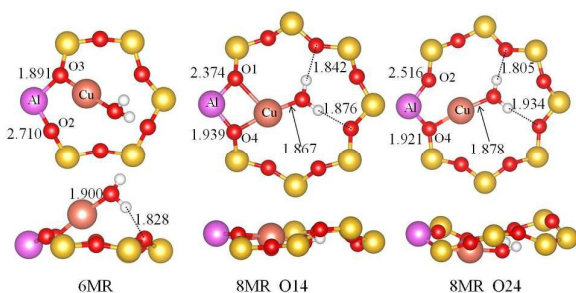
Fig. 4 Local structures of H_2O adsorbed in a ZCu conformation when Cu is located in a 6MR, a 8MR_O14, and a 8MR_O24 site. The smallest white spheres represent H atoms. The color-coding for the other spheres and the given distances have the same meaning as in Fig. 2 and 3.

presence of most adsorbates studied here. Hence, one should consider the total energy differences between Cu in the 8MR and the 6MR sites in the presence of adsorbates when comparing the stability of these adsorption sites.

In order to understand the largest total energy differences between Cu in the 8MR and the 6MR sites found during H_2O adsorption on ZCu, the local structures are further examined. As shown in Fig. 4, Cu forms strong bonds to the lattice O3, O4, and O4 atoms when Cu is located in the 6MR, 8MR_O14, and 8MR_O24 sites, respectively. There is also a weak interaction between Cu and lattice O2, O1, and O2 atoms with longer distances. The Cu also forms a bond to the O atom of the H_2O molecule with small bond distance differences between the three configurations. The two H atoms of H_2O interact with the lattice O atoms in both 8MR configurations while only one H atom of the H_2O interacts with the lattice O atom for the 6MR configuration. The different interactions between the H atoms in the H_2O molecule and the lattice O atoms results in the large total energy difference between the 8MR and 6MR configurations.

Other local structures of Cu in the 6MR, 8MR_O14, and 8MR_O24 sites with molecular adsorption are presented in Fig. S5. Note first that H_2O and NH_3 adsorption results in more complicated structures. Adsorption of both molecules results in maintenance of only one Cu—O bond with a framework O atom when Cu is in the 6MR and 8MR_O24 sites. Although Cu in the 8MR_O14 site maintains 2-fold coordinated to O atoms in the framework, the distance between Cu and one of the lattice framework O atoms is longer (2.374 and 2.346 Å for H_2O and NH_3 adsorption, respectively). Furthermore, NH_3 has a stronger interaction with Cu than H_2O, which can be seen by comparing the NH_3_ZCu and the H_2O_ZCu adsorption energies given in Table 2 when Cu is located in the 6MR and the 8MR sites. These results are consistent with the ones reported by Paolucci et al.[14]

For other molecules, binding with adsorbates also weakens the binding of Cu with the zeolite framework. In the clean ZCu conformation with Cu in the 6MR site, Cu is 3-fold coordinated to O atoms in the framework. Upon molecular adsorption, only two bonds to the O2 and O3 atoms adjacent to the Al atom are preserved. In addition, Cu moves from an almost planar position

within the 6MR to a position above the ring. For Cu in the 8MR sites, it remains 2-fold coordinated to O atoms in the framework upon molecular adsorption, which are adjacent to the Al atom. As a result, Cu maintains a coordination number of 3 upon molecular adsorption despite its location in a 6MR, a 8MR_O14, or a 8MR_O24 site. The analysis of the changes in the geometry (see Fig. S5) shows that Cu in all sites possess the same coordination number and almost the same Cu-O and Cu-M (M denotes molecule) bond lengths in the presence of adsorbates, which results in nearly identical energetic stabilities (as shown in Fig. 3) of molecularly adsorbed species in the ZCu conformation with Cu in different sites.

Molecular co-adsorption on ZCu

The molecular adsorption shown above only considers the simplest situation, i.e., adsorption of a single molecule (or OH- and NO3-) on a Cu site. Under practical NH3-SCR reaction conditions, adsorption complexes with more than one ligand on each Cu-ion site are expected. The following calculations attempt to address such complexities. Namely, NO and CO adsorption are considered under two conditions: (1) at high NO (or CO) pressure via the co-adsorption of 2 NO (or 2 CO); and (2) in the presence of other ligands (i.e., OH- and H_2O).

For the co-adsorption of 2 NO on Cu in 6MR and 8MR sites, the 2 NO molecules weaken each other's adsorption energy as compared with the adsorption of a single NO molecule. As shown in Table 3, the adsorption energies per NO of 2NO_ZCu with Cu in a 6MR, a 8MR_O14, and a 8MR_O24 site present energy differences of 0.19, 0.53, and 0.45 eV with respect to the corresponding values of NO_ZCu. Co-adsorption with OH shows that the adsorption of NO becomes slightly stronger for Cu on the 6MR site while it weakens the adsorption of NO on Cu on the 8MR sites. As shown in Fig. S8, the enhanced effect of OH on the adsorption of NO on Cu in a 6MR can be understood from the formation of HONO. Except for the formation of the N-Cu bond with a bond length of 2.045 Å, the N atom in NO also forms a bond with the O atom in OH with an N-O bond length of 1.895 Å when Cu in the 6MR site. For the NO+H_2O_ZCu conformation, H_2O coadsorption results in the weakest adsorption energy of NO, as listed in Table 3. However, as can be seen in Fig. S8, the co-adsorption of H_2O stabilizes Cu in the 8MR sites as the most favorable NO adsorption site, with total energy differences, ΔE, of -0.41 and -0.37 eV relative to the 6MR. This stabilization of the 8MR sites in the presence of H_2O is in contrast to the 2NO_ZCu and NO+OH_ZCu cases, where Cu in the 6MR site is more favorable than the 8MR sites based on the positive value of the total energy differences ΔE (see Fig. S8).

Table 3. Calculated adsorption energies of NO and CO under different conditions, namely, single molecule adsorption (M_ZCu), co-adsorption of 2 molecules (2M_ZCu), and co-adsorption of OH (M+OH_ZCu) and H_2O (M+H_2O_ZCu), according to Equation 3. Here, M represents NO or CO.

Adsorbed system	E_{ads}^{NO} (eV)			E_{ads}^{CO} (eV)		
	6MR	8MRO14	8MRO24	6MR	8MRO14	8MRO24
M_ZCu	-1.27	-1.78	-1.69	-1.60	-2.09	-1.99
2M_ZCu	-1.08	-1.25	-1.24	-0.79	-1.41	-1.42
M+OH_ZCu	-1.31	-1.03	-1.02	-0.29	-0.44	-0.41
M+H_2O_ZCu	-0.65	-0.84	-0.72	-0.94	-1.16	-0.99

The adsorption of CO presents a similar co-adsorption behavior to NO under various conditions. When compared with the adsorption of a single CO molecule, the co-adsorption of 2 CO molecules and the co-adsorption of either CO with OH or CO with H_2O results in a weakening of the adsorption energy of the CO molecule on ZCu in its three locations. As can be seen from Table 3, co-adsorption of CO with OH results in the greatest weakening effect on the interaction between CO and Cu. As shown in Fig. S8, the Cu-C bond length is longer in the CO+OH_ZCu conformation than that in the CO_ZCu conformation. Note that for the 2CO_ZCu conformation, only one CO is adsorbed on Cu in the 6MR site while the other CO molecule is located in the gas phase within the zeolite. This difference explains the very large total energy differences, ΔE, observed between 2CO_ZCu in the 8MR and 6MR sites, where the ΔE values are -0.79 and -0.76 eV for Cu in the 8MR_O14 and 8MR_O24, respectively, as compared to Cu in the 6MR site. Finally, in contrast to the NO+OH_ZCu conformation, the co-adsorption of OH with CO in the 8MR is more favorable than their co-adsorption in the 6MR site. Overall, the results of the CO+OH_ZCu calculations are consistent with previous knowledge since the interaction between Cu+ and OH results in oxidation of Cu+ to Cu2+ while the interaction between CO and Cu2+ is known to be very weak.[12,18]

Theoretical K-edge XANES of Cu in Cu-SSZ-13

As is well known, an analysis of the XANES spectra can provide a fingerprint of a particular structure for species identification.[44-49] The K-edge XANES of Cu in bulk Cu, Cu_2O, CuO, $[Cu(NH_3)_4]^{2+}$ and $[Cu(H_2O)_6]^{2+}$ are calculated first in order to verify our calculation and analysis method. The calculation details can be found in section 7 of the Supporting Information. As shown in Fig. 5a, these computational results are consistent with the experimental results,[6] demonstrating the reliability of the calculation setups used here. Please note that the computational edge position of XANES is defined here as the energy where the first derivative of the XANES intensity is maximum. However, the determination of the experimental edge position is often complicated by the presence of structured "pre-edge" and "edge-rising" peaks corresponding to transitions to an empty bound state.[44] As such, the edge position determined in Figure 5a is usually denoted as the edge-rising peak in the literature if the peak lies in the 8983-8984 eV range[44]. In addition, a direct comparison between experiment and theory with regard to the Cu K-edge XANES spectra of bulk Cu, $[Cu(NH_3)_4(H_2O)_2]^{2+}$ and $[Cu(H_2O)_6]^{2+}$ can be found in Fig. S9. Additional comparisons between these reference compounds and other possible conformations not shown in Figure 5a are made in Figure S9 as well. In particular, since the $[Cu(H_2O)_6]^{2+}$ experimental reference compound is prepared by dissolving Cu2+-nitrate with H_2O, we also compare the experimental XANES spectrum to $Cu(H_2O)_6(NO_3)_2$ in the Supporting Information[50]. Similarly, taking the Cu2+-nitrate and adding a large excess of NH_4OH synthesizes the Cu tetraamine experimental reference. As a result, we also compare the XANES spectrum for this Cu tetraamine reference compound to $Cu(NH_3)_4(NO_3)_2$ in the Supporting Information as well[51]. As for the Cu_2O and CuO reference compounds, further discussion will be
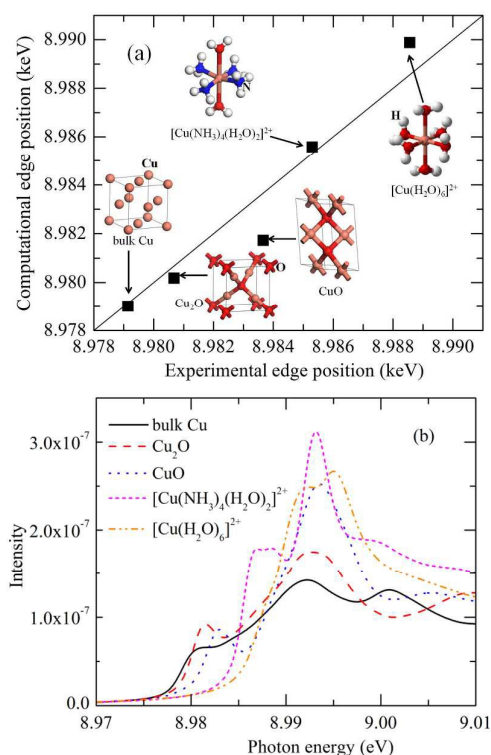

Fig. 5 (a) Comparison of the Cu XANES K-edge positions for several Cu reference species. The structures of Cu (1×1×1), Cu_2O (1×1×1), and CuO (1×1×1) unit cells, as well as the $[Cu(H_2O)_6]^{2+}$, and $[Cu(NH_3)_4(H_2O)_2]^{2+}$ species in a box of 10 Å are shown in the figure. (b) Computational results of the Cu K-edge XANES with an absolute intensity scale for different Cu reference species.

given in the following paragraph. Fig. 5b shows computational results for the Cu K-edge XANES without intensity normalization. It is found that the maximum intensity of the main peak of the Cu K-edge XANES varies with the environment surrounding the Cu species and follows this order: bulk Cu < Cu_2O < CuO < $[Cu(H_2O)_6]^{2+}$ < $[Cu(NH_3)_4(H_2O)_2]^{2+}$. As mentioned in Section 2, the XANES intensity is proportional to the probability of absorption of a photon by a core electron.[38]

Here, the XANES spectrum is analyzed by comparing it to the PDOS of Cu with a core-hole. Note that it is difficult to evaluate the transition energy by using the pseudopential method,[52] therefore, the transition energy of our Cu K-edge XANES is referenced to the Fermi level.[36] In order to compare the computational and experimental XANES on the same energy axis, a reported Cu 1s energy level of 8978.9 eV[53] is used to shift the energy axis of the computational Cu K-edge XANES. Then the energy axis is translated from relative values to the absolute ones, which is the incident photon energy in experiment.

Using Cu_2O and CuO as examples, Fig. 6 shows the experimental and computational K-edge XANES of Cu in Cu_2O and CuO, as well as the corresponding 4p PDOS of Cu in its excited state for both oxides. As shown in Fig. 6a and 6b, the Cu K-edge XANES corresponds to the 4p component of Cu with a core-hole. The 4p peak of CuO, located in the energy range spanning from 8980 to
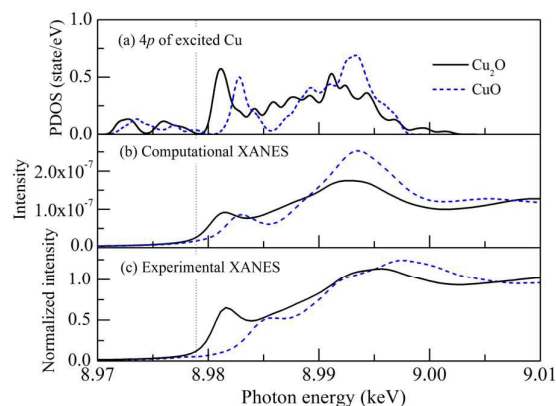
Fig. 6 (a) The 4p PDOS of Cu in its excited state (a Cu with core-hole) for the Cu$_2$O (solid line) and the CuO (dash line) oxides. The (b) computational and (c) experimental K-edge XANES of Cu in the oxides of Cu$_2$O (solid line) and CuO (dash line). The dotted line represents the Fermi level.
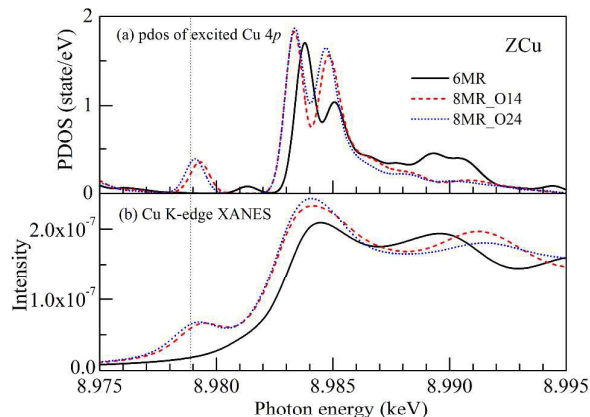

Fig. 7 The calculated (a) PDOS of excited Cu 4p and (b) computational Cu K-edge XANES and in 6MR (solid line), 8MR_O14 (dashed line), and 8MR_O24 (dotted line) locations for clean ZCu. The vertical dotted line at 8978.9 eV shows the Fermi level.

8985 eV, is at a higher energy value than that of Cu$_2$O. This correlates well with the fact that the Cu in CuO has a higher oxidation state. In addition, the intensity variation of the peaks in the Cu K-edge XANES for Cu$_2$O and CuO also correlates well with the peak heights in 4p PDOS. Although there is a slight edge position difference between the computational and experimental XANES for CuO, as shown in Fig. 6b and 6c, the computational XANES generate similar features as seen in the experimental XANES. From such a comparison of the computational Cu K-edge XANES with the experimental ones for bulk Cu, Cu$_2$O, CuO, [Cu(NH$_3$)$_4$]$^{2+}$, and [Cu(H$_2$O)$_6$]$^{2+}$, it can be concluded that the XANES calculations shown here reach good qualitative agreement with experimental results from the literature. In addition, the calculated 4p PDOS of Cu in its excited state allows one to gain further insights into XANES Cu K-edge spectra.

Several theoretical XANES results of the Cu$^+$ species will be discussed in detail, starting with the theoretical Cu K-edge XANES of clean ZCu with Cu in a 6MR, 8MR_O14, and 8MR_O24 site (see Fig. 2). As shown in Fig. 7b, there is a small peak in the 8978 to 8980 eV energy range of the XANES spectra of Cu in both the 8MR sites, which is not present in the corresponding XANES when Cu is in a 6MR site. This result is in agreement with the recent theoretical XANES modeled by Lamberti and coworkers.[45] The "white line" position in the XANES spectra of Cu in the 6MR site is higher than that of Cu in the 8MR sites by a small energy difference of ~0.5 eV. On the other hand, the XANES edge position of Cu in the 6MR and 8MR sites nearly overlap. As a result, the presence of the small peak feature for Cu in the 8MR sites does not necessarily correlate with Cu in a Cu$^+$ oxidation state, as was previously inferred in the literature when analyzing the experimental XANES spectra.[6] Rather, it is the edge position that correlates well with the oxidation state of Cu in the different sites, since both Cu species in the 6MR and the 8MR as examined here have the same oxidation state and the same edge position.

The Cu XANES spectra difference can be correlated to a 4p PDOS analysis of the excited states of Cu within the empty band region, as shown in Fig. 7a. The 1s to 4s and 1s to 3d transitions are forbidden from the dipole selection rules.[26] Therefore, the PDOS of 4s and 3d

states are not displayed in Fig. 7a. As done above, the energy scale of the PDOS with respect to the Fermi level is shifted in order to clearly correlate the 4p PDOS and XANES spectra. There is an energy gap between the small peak around 8980 eV and the main peak around 8984 eV of the 4p states. However, the gap in the 4p states for Cu in the 8MR sites is larger as compared to when Cu is located at the 6MR. In addition, the small peak features in the 4p PDOS for Cu in the 8MR sites are larger than those in the 6MR site. As a result, the small peak feature in the XANES spectra when Cu is located in a 8MR site is generated by a 1s to 4p transition while the XANES of Cu in a 6MR does not have such a small lower-energy lying peak. It is concluded that the presence of the small peak feature around 8980 eV in the theoretical XANES results originates from the small peak in the 4p PDOS, which is non-negligible when Cu is located in one of the 8MR sites.

Furthermore, the orbital distribution of the different peaks when Cu is located in the 6MR and the 8MR sites is analyzed, as displayed in Fig. 8. As shown in Fig. 7, no apparent difference is found between the two 8MR sites with respect to their PDOS and XANES.
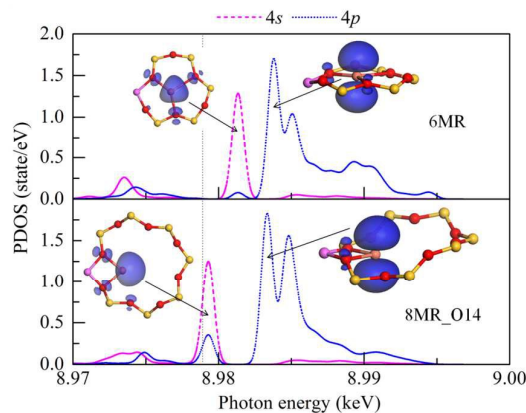

Fig. 8 The PDOS of Cu in its excited state. The PDOS of the 4s (dashed line) and 4p (dotted line) states are plotted. The iso-surface value of the orbital distribution is 0.04 electrons/Å^3. The vertical dotted line at 8978.9 eV presents the Fermi level.
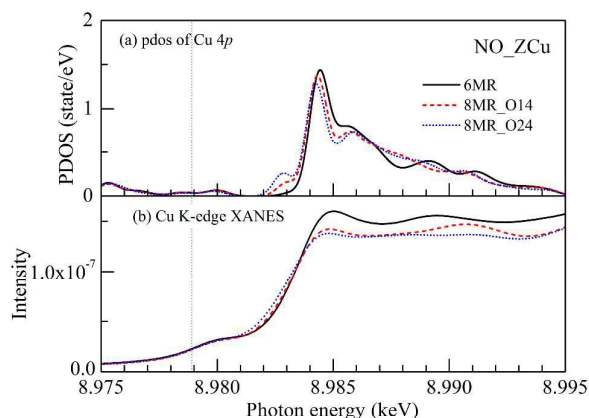
Fig. 9 The calculated (a) PDOS of excited Cu 4*p* and (b) computational K-edge XANES of Cu in 6MR (solid line), 8MR_O14 (dashed line), and 8MR_O24 (dotted line) locations for NO_ZCu. The vertical dotted line at 8978.9 eV shows the Fermi level.

Therefore in Fig. 8, only the PDOS for Cu in 8MR_O14 is shown to compare with that for Cu in the 6MR site. This confirms that the Cu 4*p* state contributes significantly to the main peak around 8984 eV when Cu in located in the 6MR and the 8MR, where the orbital distributions shown in Fig. 8 correlates well with that of a $4p_z$ orbital. The different contributions of the 4*p* state for Cu in the 6MR and 8MR site affects the orbital shape, as shown in the left inset of Fig. 8: the orbital distribution of Cu in the 6MR is more symmetrical than that of Cu in 8MR. These results imply that the XANES features are also influenced by the coordination number and geometry of the Cu ion.

Upon NO adsorption, the Cu K-edge position becomes independent of the Cu location, as shown in Fig. 9b. This correlates well when comparing the NO_ZCu structures shown in Fig. S5. Indeed, in each configuration the Cu is 3-fold coordinated and bound to two lattice O atoms and the N atom of the NO molecule.
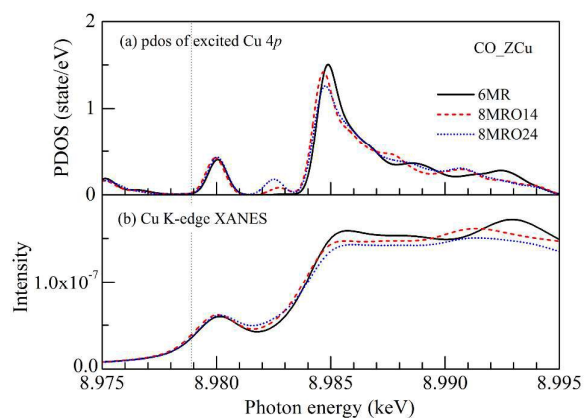

Fig. 10 The calculated (a) PDOS of excited Cu 4*p* state and the corresponding (b) K-edge XANES of Cu in the 6MR (solid line), 8MR_O14 (dashed line), and 8MR_O24 (dotted line) site for the CO_ZCu conformation. The vertical dotted line at 8978.9 eV is the Fermi level.

The Cu-O and Cu-N bond lengths vary only slightly when the Cu locations change, as shown in Fig. S5. In addition, the 4*p* empty state of Cu is also independent of the Cu locations, as shown in Fig. 9a. These results demonstrate that upon NO adsorption, Cu in the 6MR and 8MR sites have the same oxidation state and nearly identical chemical environment. This is in contrast to when a bare Cu is located in the 8MR and the 6MR, where the coordination numbers differ for Cu-ions in the two locations. As shown in Fig. 9b, a small shoulder around 8980 eV also appears in the K-edge XANES of Cu. This shoulder can be assigned to the small peak found in the 4*p* PDOS in the same energy range, which becomes convoluted with the main peak around 8984 eV when one computes the corresponding XANES spectra. Note also that the intensities of the main XANES peak correlate very well with the corresponding peak heights in the 4*p* PDOS.

An identical analysis is applied to ZCu with CO adsorption on Cu. The results of the Cu K-edge XANES and the excited Cu 4*p* states for the CO_ZCu configurations are shown in Fig. 10. In this case, the small peak feature around 8980 eV of the Cu K-edge XANES correlates nicely with the 4*p* states peak. Because CO and N_2 molecules have similar electronic structures, the Cu K-edge XANES of CO_ZCu and N_2_ZCu appear similar, even though CO binds more strongly to the Cu site than N_2 (Table 2). Results for the Cu K-edge XANES and PDOS empty band for N_2_ZCu can be found in Fig. S10.

By analyzing the orbital distribution, further insight into the origin of the small peak around 8980 eV in the XANES can be gained, as shown in Fig. 11. Fig. 11a displays the PDOS of the 2*p* state for CO and the exited 4*p* state for Cu in the CO_ZCu conformation, as well as the corresponding orbital distribution. Because the XANES and the PDOS of Cu in the CO_ZCu conformation are independent of the Cu location, only the analysis for Cu in an 8MR site is shown. It is found that the splitting of the 4*p* state of Cu is induced by the interaction between Cu and the CO molecule. Specifically, the 2π* orbital of CO induces a peak in the 4*p* state distribution for Cu close to the Fermi level, which is reflected by a small peak around 8980 eV in XANES. Experimentally, the Cu K-edge XANES spectra in the presence of CO under different conditions were measured.[18] Fig. 11b shows the experimental XANES spectrum of the CO-reduced Cu-SSZ-13 sample in a CO/He stream at 25°C. The weak feature centered around 8980 eV found experimentally has been proposed to represent the Cu$^+$ ions containing CO in their coordination environment.[18] Using the simple model structure of CO_ZCu shown in Fig. 11b, this feature is reproduced computationally. This progress achieved on understanding the computational Cu K-edge XANES by the PDOS and orbital distribution of Cu ions can, therefore, be used to better understand the features found in the experimental XANES. It is important to remark, however, that experimentally it is difficult to obtain a Cu-SSZ-13 sample with only Cu$^+$ sites. The fact that the white line intensity and shape of computational XANES is not identical to the experimental one, may be understood from the presence of Cu^{2+} in practical Cu-SSZ-13 samples. In addition, the modelling limitations could also have a significant impact on the direct comparison between computational and experimental XANES.[54]
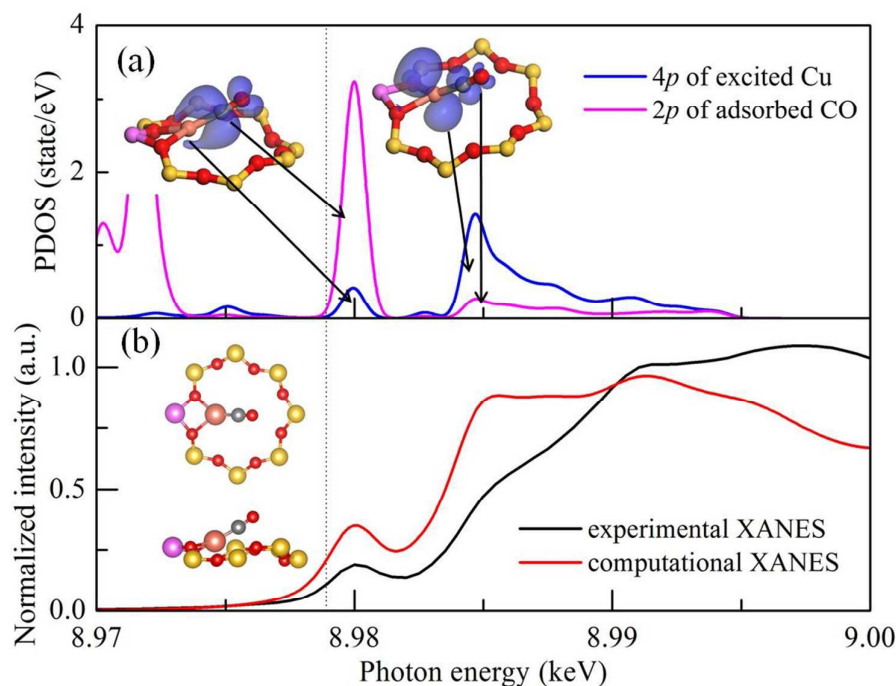
Fig. 11 (a) The PDOS of the 2p state of CO and the *4p* state for the excited Cu in the CO_ZCu conformation when Cu is located in an 8MR_O14. The orbital distributions of the peaks in the PDOS are also shown. The iso-surface value is 0.04 electrons/Å^3. The dotted line at 8978.9 eV is the Fermi level. (b) Comparison of the computed XANES spectrum for the structure model shown in the inset (CO_ZCu with Cu in 8MR_O14) and the experimental XANES spectrum of the CO-reduced Cu-SSZ-13 sample in a CO/He stream at 25°C.[18]

As shown in Figs. 7, 9, and 10, the peak intensity maxima in the Cu K-edge XANES vary slightly with the different Cu locations. Among all the ZCu systems studied, the H_2O_ZCu and NH_3_ZCu systems show the largest intensity variations for different Cu locations, as shown in Figs. 12 and 13. In the H_2O_ZCu configuration, the maximum intensity of the Cu K-edge peaks in the 6MR and 8MR_O24 sites are almost twice that of Cu in the 8MR_O14 site. The edge positions also vary slightly with different Cu locations, which are 8983.12, 8983.48, and 8983.29 eV for Cu in 6MR,

8MR_O14, and 8MR_O24 sites, respectively. The edge position shifts with respect to Cu in a 6MR site are 0.36 and 0.17 eV for Cu in an 8MR_O14 and an 8MR_O24 site, respectively. Note that such small changes in edge position may not be of practical significance since experimental resolutions for XANES are only about ~1 eV. K-edge peak intensity differences caused by configuration variations are more important here.

On the another hand, the XANES spectra of the NH_3_ZCu conformation with Cu located in an 8MR_O14 and an 8MR_O24 site are almost identical; while having Cu in a 6MR site results in the
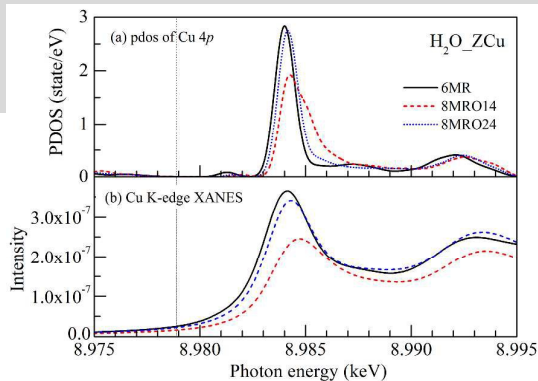

Fig. 12 The calculated (a) PDOS of the Cu 4*p* exited state and the computational (b) K-edge XANES of Cu in the 6MR (solid line), the 8MR_O14 (dashed line), and the 8MR_O24 (dotted line) locations for the H_2O_ZCu conformation. The vertical dote line at 8978.9 eV shows the Fermi level.
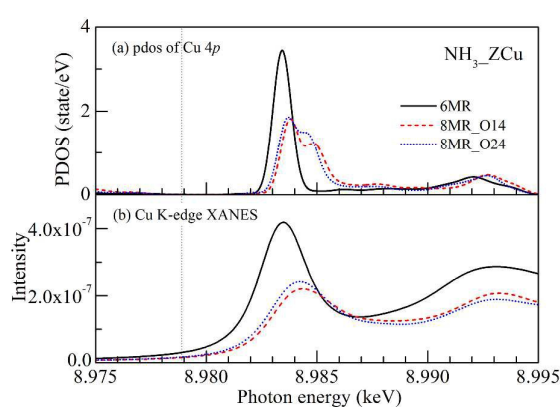

Fig. 13 The calculated (a) PDOS of Cu 4*p* exited state and the computational (b) K-edge XANES of Cu in the 6MR (solid line), 8MR_O14 (dashed line), and 8MR_O24 (dotted line) locations for the NH_3_ZCu conformation. The vertical dotted line at 8978.9 eV shows the Fermi level.

largest peak intensity, as shown in Fig. 13. Such a strong peak intensity is consistent with several experimental XANES studies on ammonia adsorption on Cu-zeolites that were reported in the literature.[14, 46, 47] The edge position of the NH_3_ZCu conformations shifts with different Cu locations with extents of 0.57 and 0.48 eV when comparing the edge position of the 6 MR to the 8MR_O14 and the 8MR_O24 Cu sites, respectively. It is also found that the white line of the Cu K-edge XANES for the NH_3_ZCu conformation is located at a photon energy of around 8983 eV.

A number of insights can be gained into the H_2O_ZCu and NH_3_ZCu XANES results through an analysis of the corresponding PDOS for the excited Cu $4p$ state, as shown in Fig. 12a and 13a. Therefore, in addition to the variation of the edge position, the intensity of the maximum peak is also an important parameter since it varies with the location of Cu.

The strong intensity of the peak around 8983 eV in XANES for H_2O_ZCu (or NH_3_ZCu) is due to the linear configuration of the Cu^+ ion. In the literature, it is known that for the Cu^+ ion with a linear configuration has an unusually high edge-rising peak, which surpasses the intensity of white line around 8994 eV.[10, 47, 48, 49] Indeed, in a study of Cu-sites in metalloproteins by Kau et al., it was found that the high intensity of the edge-rising peak is because of the doubly degenerate $4 p_{xy}$ final state while the white line is a 1s to $4 p_z$ transition.

Representative Cu K-edge XANES in the presence of HONO, N_2O, NO_2, NO_3^-, O_2, and OH^- can be found in Fig. S11. It is found that the edge position and intensity of the maximum peak of the Cu K-edge XANES depends both on the Cu locations and the nature of the adsorbed molecules. Finally, it is worthwhile noting that our computational XANES results for the NO_2_ZCu and NO_3_ZCu conformations, as shown in Fig. S11, have a shoulder peak around 8986 eV, which are consistent with the experimental XANES reported by Beato and coworkers.[10]

Next, the computational XANES for Cu-SSZ-13 with various chemisorbed model species are compared to the experimental spectra obtained under standard and fast SCR conditions. Fig. 14a shows an experimental XANES spectra of 2.1 wt.% Cu-SSZ-13 under standard and fast SCR conditions at 473 K. Details of the experimental procedure can be found elsewhere.[6] The main difference between the XANES under standard and fast SCR conditions is that there is a peak around 8982.5 eV in the XANES spectrum under standard SCR conditions while there is no corresponding peak under fast SCR conditions. As described in the literature,[6] several structures were assigned to the different peaks. As shown in Figs. 14b and 14c, the computed Cu K-edge positions for the H_2O_ZCu and $2OH\_ZCu$ structures correlate well with the features in the XANES spectra that were assigned previously[6]: the edge positions of the Cu^{2+} species for the $2OH\_ZCu$ structure is located at a higher energy than that of the Cu^+ species for the H_2O_ZCu structure. Furthermore, more possible configurations of
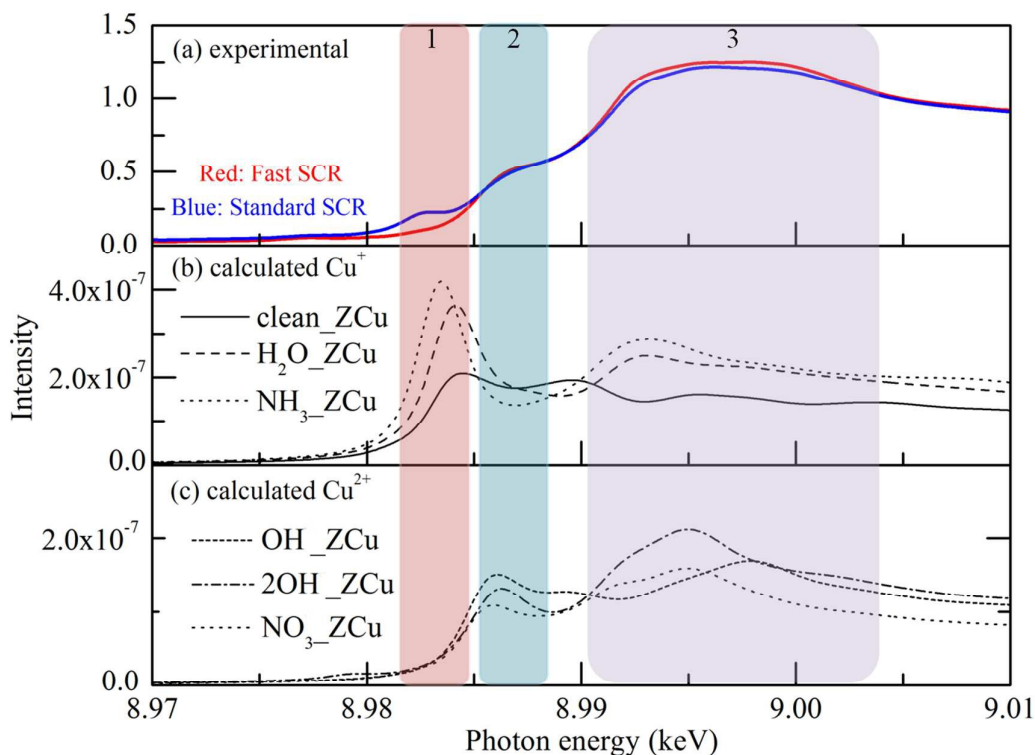

Fig. 14 (a) Experimental Cu K-edge XANES of 2.1 wt.% Cu-SSZ-13 under standard and fast SCR conditions at 473 K.[6] The three peak regions labeled as 1, 2, and 3 are shaded to guide the eyes. Computational Cu K-edge XANES of different (b) Cu^+ and (c) Cu^{2+} species in the 6MR site.

12 | *Catal. Sci. Technol.*, 2015, **00**, 1-15

This journal is © The Royal Society of Chemistry 20xx

clean_ZCu and NH_3_ZCu for Cu^+ species, OH_ZCu and NO_3_ZCu for Cu^{2+} species are considered. The calculated Cu K-edge XANES for these structures are also shown in Fig. 14b and Fig. 14c. When examining all these possibilities, it is found that the main contribution to the peak in region 1 of the experimental XANES spectrum under standard SCR conditions is mainly due to Cu^+ species with linear coordination geometries. In particular, the simulated XANES the H_2O_ZCu and NH_3_ZCu conformations have a very strong peak around 8.983 keV, where the intensity is two times stronger than that of a "bare" ZCu (the main peak in Fig. 7). The regions marked 2 and 3 in Fig. 14a have almost the same experimental features under standard and fast SCR conditions. As can be seen from Fig. 14c, the main contributions to these regions are from our model Cu^{2+} species under chemisorption conditions. Therefore, these results support the conclusion that mixed Cu^+ and Cu^{2+} oxidation states are present under standard SCR conditions while Cu^{2+} species dominate under fast SCR conditions.[6] Note that the present study only focuses on Cu sites charge compensated with a single Al atom. For the situation where Cu is charge compensated by two Al atoms, other possible Cu^{2+} species could also contribute to regions 2 and 3.

Our computational XANES results also provide an alternative explanation of the experimental results that the reduction of Cu in the presence of NH_3 and NO is characterized by an strong peak around 8983 eV.[10] Indeed, by comparing the XANES spectrum in of a bare Cu^+ ion and that of a Cu^+ ion in the presence of NH_3, no change in the oxidation state of Cu is observed. However, there is indeed a dramatic increase in the peak height around 8983 eV when NH_3 is present. Similar observations in experimental XANES have been attributed to an increase in the number of Cu^+ sites in the presence of NH_3.[14, 46] The computational results, however, show that the XANES intensity is sensitive not only the oxidation state of the Cu ion but also to the nature of the adsorbates since this equally alters the corresponding PDOS. More importantly, the linear coordination geometry and coordination number of Cu ion determine the high intensity of the peak around 8983 eV for a Cu^+ ion.[48,49] As a result, the simultaneous presence of such an edge-rising transition at 8983 eV complicates the reliable determination of the edge position and hence a determination of the oxidation state of Cu. For this reason, a robust experimental tracking of the Cu oxidation state is often done also by monitoring of the weak dipole-forbidden pre-edge peak at 8978 eV,[44] mostly rising from 1s to 3d transition in Cu^{2+}. Although such dipole-forbidden transitions are not taken into account here in our calculations, experimentally it represents an unambiguous fingerprint for the presence of Cu^{2+} in the probed system.

To further mimic experimental conditions,[17, 18] the Cu K-edge XANES of the ZCu conformation in the presence of several NO (or CO) species were investigated. In addition, the influence of other common ligands (i.e., OH and H_2O) on the XANES spectrum was also investigated. The comparison of the Cu K-edge XANES for the clean ZCu, NO_ZCu, 2NO_ZCu, NO+OH_ZCu, and NO+H_2O_ZCu conformations are displayed in Fig. 15, where Cu is located in the 6MR and the 8MR_O14 site with the corresponding conformations given in Fig. S8. Spectra for Cu located in the 8MR_O24 site are shown in the Supporting Information.
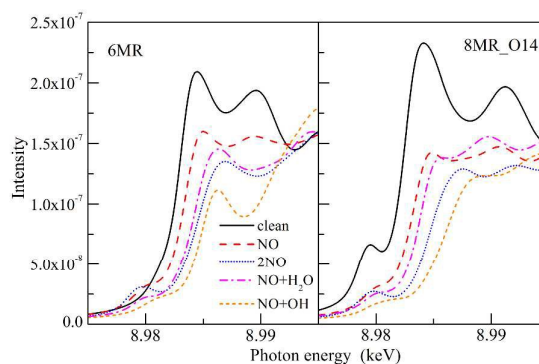

Fig. 15 The K-edge XANES of Cu in several ZCu conformations with different Cu locations (6MR and 8MR_O14) under different situations, namely, clean, NO adsorption, 2NO adsorption, co-adsorption of NO with water, and co-adsorption of NO with OH The same plot for Cu in 8MR_O24 can be found in Fig. S12.

In spite of the different Cu locations, adsorption of additional species generally results in a shift of the edge position and the white line to higher energies and a decrease of the intensity of the white line. The edge position follows this order (from low to high energy): clean < NO < NO+H_2O < 2NO < NO+OH. In particular, the adsorption of 2 NO molecules results in a shift in the edge position of the Cu K-edge XANES to higher energy, as compared to the NO_ZCu conformation, where the energy shifts are 1.12 and 1.34 eV for Cu in the 6MR and 8MR_O14 sites, respectively. The NO+OH_ZCu conformation represents a situation where Cu presents as Cu^{2+}.[22] When considering different Cu locations for the NO+OH_ZCu conformation, the edge position of Cu in a 8MR site is at a higher energy than that in a 6MR site, where the edge position difference is 1.24 eV.

CO is an important probe molecule in studying Cu-SSZ-13. Recently, Kwak _et al._ collected Cu K-edge XANES spectra during calcinations, reduction with CO, and adsorption of CO and H_2O on Cu-SSZ-13.[18] The results show a variation in the oxidation states of the copper species in the zeolite structure, and provide information on the changes in the coordination environment around Cu ions as they interact with the framework and with different adsorbates
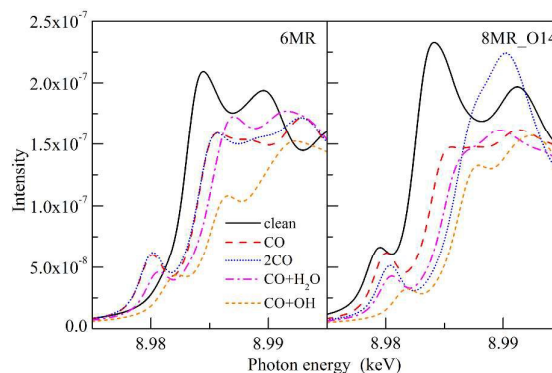

Fig. 16 The K-edge XANES of Cu for the ZCu systems with different Cu locations (6MR and 8MR_O14) under different situations, namely, clean, CO adsorption, 2CO adsorption, co-adsorption of CO with water, and co-adsorption of CO with OH. The same plot for Cu in 8MR_O24 can be found in Fig. S13.

(H_2O and CO). Analogous computational studies of the Cu K-edge XANES were performed for the ZCu system with varying amounts of CO, as shown in Fig. 16. The influence of water on the XANES spectrum was also investigated. Similar overall conclusions for the NO system can be applied to the CO studies except when 2 CO molecules are adsorbed on a Cu ion in 6MR site. As mentioned previously, only one CO molecule was adsorbed on Cu when it is located in a 6MR site when the 2CO_ZCu conformation was examined, while the other CO molecule does not bind to the zeolite framework or the Cu ion. Consequently, the same XANES was obtained for the CO_ZCu and 2CO_ZCu configurations with Cu in the 6MR site. Another interesting difference between the NO and the CO system is that the presence of CO results in a more prominent small peak feature around 8980 eV in the XANES spectrum, for which its decrease in intensity correlates well with the shift of the edge position. Experimentally, during the procedure of reduction with CO on calcined Cu-SSZ-13, the edge position decreases with a decreasing Cu oxidation state.[18] Kwak *et al.* proposed that the Cu^+ ions represented by the XANES feature at 8980.5 eV are ones that contain CO in their coordination environment while the feature at 8982 eV originates from a CO-free Cu^+ ion. The computational XANES for CO_ZCu with the small peak around 8980 eV (Fig. 11 and 16) and the peak at 8982 eV for clean_ZCu (Fig. 7) confirm these experimental assignments. In addition, the co-adsorption of CO with H_2O on Cu ions causes the small peak feature at 8980 eV and its edge (or edge-rising) position to shift to higher photon energies. Taking Cu in an 8MR_O14 site as an example, in presence of H_2O (CO+H_2O_ZCu), the 8980 eV feature and edge position shift to higher energies by 0.46 and 1.00 eV, respectively, compared with those of CO_ZCu. This result is in good agreement with the experimental findings that the accumulation of H_2O on Cu ions lead to a shift of the spectra to higher photon energies.[18]

Next, several species (H_2O, O atom, O_2, OH, and 2OH) with different oxidizing potential are used to examine the relationship between the molecular ligand and the Cu XANES edge position. As
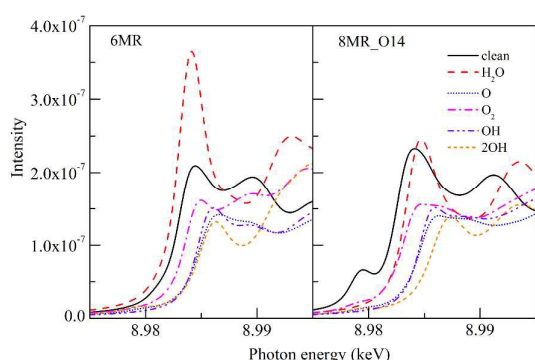
Table 4. Edge position shifts in the Cu K-edge XANES in the presence of several adsorbates in the ZCu conformation (as shown in Fig. 17) with respect to the corresponding clean ZCu conformation with different Cu locations. The original data of the edge positions can be found in Table S4. As the resolution of the computational XANES is 0.05 eV, H_2O does not change the edge position of Cu located in a 6MR site.

Shift of edge position (eV)	clean	H_2O	O_2	O	OH	2OH
6MR	0.00	0.02[a]	0.62	1.76	1.63	1.90
8MR_O14	0.00	0.88	0.67	2.11	2.11	3.20
8MR_O24	0.00	0.70	0.70	2.21	2.22	3.24

[a]Note that for Cu in the 6MR site, Fig. 17 shows that the Cu edge position in the ZCu conformation in the presence of H_2O appears to be at a lower energy than that of the clean ZCu conformation. However, the calculated result in Table 4 shows that the edge position of H_2O adsorbed on ZCu is essentially the same with that of the clean ZCu conformation. The reason for the positive edge shift (displayed visually in Fig. 17) is due to the higher intensity of Cu K-edge XANES for H_2O adsorbed on a Cu^+ ion as compared to the clean ZCu conformation, which alters the edge position.

can be seen by examining Fig. 17, the edge positions vary noticeably in the presence of different species, and also display a weak dependence on the Cu locations. Adsorption of H_2O results in a more complicated situation because of the interaction between H_2O and the lattice O, as discussed previously. Overall one can see in Fig. 17 that the adsorption of such species results in a shift of the edge position to higher energies. The XANES edge shifts with respect to the corresponding clean ZCu conformations are listed in Table 4 for Cu in different locations. In addition, the largest shifts are realized when Cu is in one of the 8MR sites with adspecies having strong oxidizing potentials (O, OH, and 2OH). This conclusion is in complete agreement with the reported experimental DRIFTS/XANES results,[18] where it was concluded that Cu^{2+} ions in 6MR were much more difficult to reduce to Cu^+. Specifically, in the reduction experiment with a gas mixture of 1% CO/He in the 25~400°C temperature range, it was not possible to reduce Cu^{2+} ions in 6MR while Cu^{2+} ions located in the 8MR were readily reduced to Cu^+.[18]

Finally, computational and experimental XANES results during a dehydration process of hydrated Cu-SSZ-13 are presented, where the experimental results were published recently by Kwak *et al.*.[18] To model a fully hydrated Cu^{2+} ion, a Cu ion that is surrounded by six H_2O water molecules and charge compensated by two Al atoms within the same 6MR is used, which is denoted herein as the H_2O_6_Z_2Cu conformation. The Z_2Cu notation denotes Cu^{2+} charge balanced by two negative framework charges, and the H_2O_6_Z_2Cu structure can be found in Fig. S15. Experimentally, the Cu-SSZ-13 sample was calcined by increasing the temperature from 25 to 400 °C in a flowing O_2/He stream. The experimental XANES spectra of the Cu-SSZ-13 sample at 25 and 400 °C are shown in Fig. 18a. The O_ZCu and the OH_ZCu model structures are used here to gain further insights into the XANES spectra of the oxidized Cu-SSZ-13 sample. The computational XANES of the H_2O_6_Z_2Cu, O_ZCu, and OH_ZCu models are shown in Fig. 18b. The peak around 8988 eV in the XANES of the H_2O_6_Z_2Cu model shifts to 8986 eV for the O_ZCu and OH_ZCu model structures. This result is consistent with the experimental result that the position of the K-edge feature observed at 8987.5 eV in the fully hydrated Cu-SSZ-13 shifts to lower energies by 2.4 eV at 400 °C. Note also that the signal
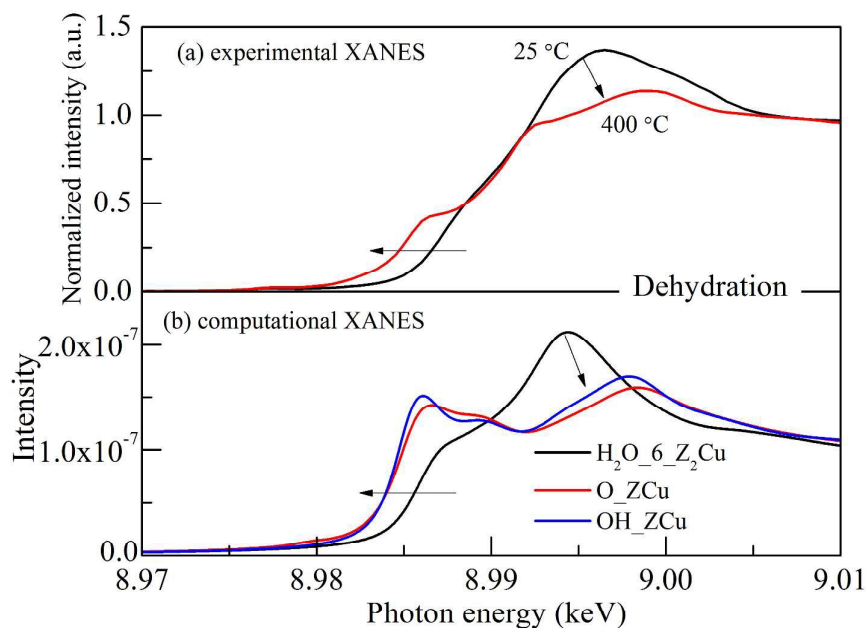

Fig. 17 The K-edge XANES of Cu in various ZCu conformations with different Cu locations (6MR and 8MR_O14), in the presence of several adsorbates (H_2O, O atom, O_2, OH, and 2OH) with different oxidizing power. The same plot for Cu in 8MR_O24 can be found in Fig. S14.

Fig. 18 (a) The experimental XANES of Cu-SSZ-13 sample at 25 and 400 °C. The sample at 25°C is fully hydrated while flowing an O_2/He stream oxidizes the sample at 400 °C. (b) The computational XANES of the corresponding $H_2O\_6\_Z_2Cu$, O_ZCu and OH_ZCu model structures. The arrows show the XANES changes during the process of oxidation.

intensity drop of the 8995 eV feature during hydration found experimentally is fully reproduced computationally.

Conclusions

In summary, several possible adsorption locations for Cu in a ZCu conformation within the zeolite framework, along with the effect of the adsorption of reactants, intermediates, and products that are present throughout the NH_3 SCR cycle, were examined using DFT calculations, and the resulting XANES were compared with available experimental results. Three possible Cu positions were considered, namely, the 6MR, 8MR_O14, and 8MR_O24 locations. The most energetically favorable site for bare Cu ions was the 6MR site, while the 8MR_O14 and 8MR_O24 sites were less favorable. However, the Cu ions in different sites of the ZCu conformations present similar chemical properties with regard to their energetics because of the insignificant *d*-band center differences. Upon molecular adsorption, the energy differences between Cu in the 8MR and 6MR sites decrease and almost disappear, except for the adsorption of H_2O. This suggests that the thermodynamic stability of molecularly adsorbed ZCu is nearly identical for Cu in different sites in the presence of adsorbates. The different adsorption behavior of H_2O with Cu in either a 6MR or a 8MR is a result of the different interactions between the H atoms of the adsorbed H_2O molecule and the lattice O atoms. Also, all of the molecules adsorbed on the Cu^+ ion in the 8MR sites present stronger adsorption energies than that of a Cu^+ ion in the 6MR site.

The results from more complex conditions (e.g. high pressure) show that increasing the NO pressure weakens Cu-NO interactions for Cu-ions in different locations, with the Cu^+ ion in the 6MR site being identified as the most favorable site. In the presence of 2 CO

molecules, the adsorption energy of each CO molecule is also weakened, with the 8MR sites being the most favorable because only one CO can adsorb on Cu^+ located in the 6MR site. The co-adsorption of NO and OH, NO and H_2O, CO and OH, as well as CO with H_2O, all results in a weakening of these species' adsorption energies, except for the NO+OH_ZCu conformation with Cu in the 6MR site. In this case, NO and OH interact to form an adsorbed HONO molecule. Overall, our energetic stability analyses of the NO+H_2O_ZCu, CO+OH_ZCu, and CO+H_2O_ZCu conformations show that the 8MR sites are more favorable than the 6MR site.

The theoretical core-level spectroscopy simulation results of Cu in the ZCu conformation allow for attribution of the small peak in the Cu K-edge XANES of a "naked" Cu+ ion in a 8MR site to a 1s to 4p transition. In the K-edge XANES of Cu in a clean ZCu conformation, a weak feature at ~8979.5 eV is found when Cu is located in a 8MR site while no such feature is observed when the Cu ion is located in a 6MR site. This difference is rationalized by analyzing the corresponding PDOS of Cu while taking into account the core-hole effect. Upon the adsorption of different species (except for H2O and NH3), the K-edge XANES cannot be used to distinguish between the Cu location/oxidation state in the presence of adsorbates since the Cu in the 6MR and 8MR sites have essentially identical chemical environments. For H2O and NH3 adsorbed on ZCu, the Cu location was found to have a strong effect on the white line intensity in Cu K-edge XANES. When NO (or CO and N2) is adsorbed onto Cu in ZCu, a small feature around 8980 eV arises in the K-edge XANES, which is induced by the splitting of the Cu 4p state. An analysis of the orbital distribution of the CO_ZCu conformation showed that the 2π* orbital induces a small peak around 8980 eV in the 4p PDOS of Cu. Molecular co-adsorption on ZCu shows that the Cu K-edge position follows the order (from low to high energy): clean < M <

This journal is © The Royal Society of Chemistry 20xx

Catal. Sci. Technol., 2015, **00**, 1-15 | **15**

M+H2O < 2M < M+OH (M denotes NO or CO). Finally, the XANES spectrum of a fully hydrated Cu-SSZ-13 catalyst was simulated and was found to be consistent with experimental results.
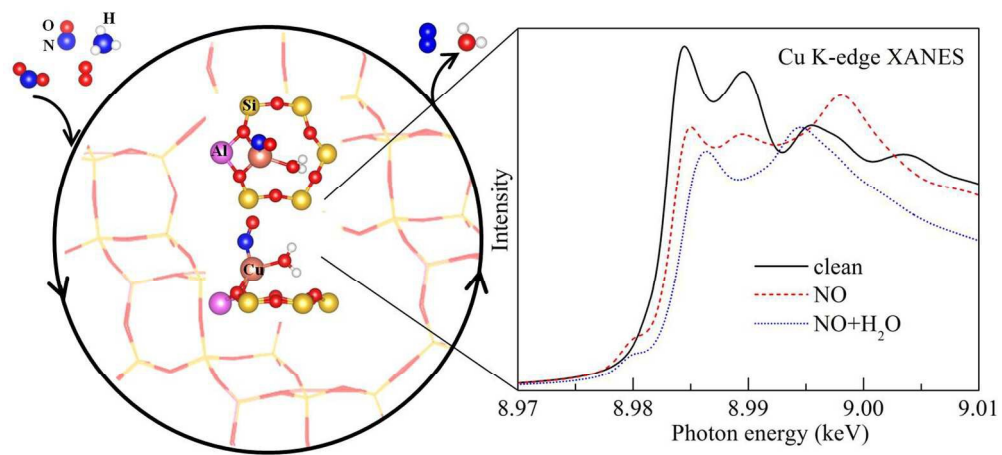
Acknowledgements

Notes and references

1   U. Deka, I. Lezcano-Gonzalez, B.M. Weckhuysen, A.M. Beale, *ACS Catal.*, 2013, **3**, 413-427.
2   S.i. Matsumoto, *CATTECH*, 2000, **4**, 102-109.
3   J.H. Kwak, R.G. Tonkyn, D.H. Kim, J. Szanyi, C.H.F. Peden, *J. Catal.*, 2010, **275**, 187-190.
4   J.H. Kwak, D. Tran, S.D. Burton, J. Szanyi, J.H. Lee, C.H.F. Peden, *J. Catal.*, 2012, **287**, 203-209.
5   D.W. Fickel, R.F. Lobo, *J. Phys. Chem. C*, 2010, **114**, 1633-1640.
6   J.S. McEwen, T. Anggara, W.F. Schneider, V.F. Kispersky, J.T. Miller, W.N. Delgass, F.H. Ribeiro, *Catal. Today*, 2012, **184**, 129-144.
7   V.F. Kispersky, A.J. Kropf, F.H. Ribeiro, J.T. Miller, *Phys. Chem. Chem. Phys.*, 2012, **14**, 2229-2238.
8   Y. Itho, S. Nishiyama, S. Tsuruya, M. Masai, *J. Phys. Chem.*, 1994, **98**, 960-967.
9   F. Gao, E.D. Walter, M. Kollar, Y. Wang, J. Szanyi, C.H.F. Peden, *J. Catal.*, 2014, **319**, 1-14.
10 T.V.W. Janssens, H. Falsig, L.F. Lundegaard, P.N.R. Vennestrøm, S.B. Rasmussen, P.G. Moses, F. Giordanino, E. Borfecchia, K.A. Lomachenko, C. Lamberti, S. Bordiga, A. Godiksen, S. Mossin, P. Beato, *ACS Catal.*, 2015, **5**, 2832-2845.
11 J.H. Kwak, J.H. Lee, S.D. Burton, A.S. Lipton, C.H.F. Peden, J. Szanyi, *Angew. Chem. Int. Ed.*, 2013, **125**, 10169-10173.
12 F. Gao, J. Kwak, J. Szanyi, C.F. Peden, *Top. Catal.*, 2013, **56**, 1441-1459.
13 X. Yang, Z. Wu, M. Moses-Debusk, D.R. Mullins, S.M. Mahurin, R.A. Geiger, M. Kidder, C.K. Narula, *J. Phys. Chem. C*, 2012, **116**, 23322-23331.
14 C. Paolucci, A.A. Verma, S.A. Bates, V.F. Kispersky, J.T. Miller, R. Gounder, W.N. Delgass, F.H. Ribeiro, W.F. Schneider, *Angew. Chem. Int. Ed.*, 2014, **53**, 11828-11833.
15 U. Deka, A. Juhin, E.A. Eilertsen, H. Emerich, M.A. Green, S.T. Korhonen, B.M. Weckhuysen, A.M. Beale, *J. Phys. Chem. C*, 2012, **116**, 4809-4818.
16 S.A. Bates, A.A. Verma, C. Paolucci, A.A. Parekh, T. Anggara, A. Yezerets, W.F. Schneider, J.T. Miller, W.N. Delgass, F.H. Ribeiro, *J. Catal.*, 2014, **312**, 87-97.
17 A.A. Verma, S.A. Bates, T. Anggara, C. Paolucci, A.A. Parekh, K. Kamasamudram, A. Yezerets, J.T. Miller, W.N. Delgass, W.F. Schneider, F.H. Ribeiro, *J. Catal.*, 2014, **312**, 179-190.
18 J.H. Kwak, T. Varga, C.H.F. Peden, F. Gao, J.C. Hanson, J. Szanyi, *J. Catal.*, 2014, **314**, 83-93.
19 S.T. Korhonen, D.W. Fickel, R.F. Lobo, B.M. Weckhuysen, A.M. Beale, *Chem. Commun.*, 2011, **47**, 800-802.
20 F. Gao, E.D. Walter, E.M. Karp, J. Luo, R.G. Tonkyn, J.H. Kwak, J. Szanyi, C.H.F. Peden, *J. Catal.*, 2013, **300**, 20-29.
21 J. Hun Kwak, H. Zhu, J.H. Lee, C.H.F. Peden, J. Szanyi, *Chem. Commun.*, 2012, **48**, 4758-4760.
22 R. Zhang, J.-S. McEwen, M. Kollár, F. Gao, Y. Wang, J. Szanyi, C.H.F. Peden, *ACS Catal.*, 2014, **4**, 4093-4105.
23 A.M. Beale, F. Gao, I. Lezcano-Gonzalez, C.H.F. Peden, J. Szanyi, *Chem. Soc. Rev.*, 2015, **44**, 7371-7405
24 J. Szanyi, J.H. Kwak, H. Zhu, C.H.F. Peden, *Phys. Chem. Chem. Phys.*, 2013, **15**, 2368-2380.
25 G.T. Palomino, S. Bordiga, A. Zecchina, G.L. Marra, C. Lamberti, *J. Phys. Chem. B*, 2000, **104**, 8641-8651.
26 S.-P. Gao, J.P. Chris, P. Alexander, M. Victor, *J. Phys. Conden. Matter*, 2009, **21**, 104203.
27 G. Kresse, J. Furthmüller, *Phys. Rev. B*, 1996, **54**, 11169.
28 G. Kresse, J. Hafner, *Phys. Rev. B*, 1993, **47**, 558.
29 P.E. Blöchl, *Phys. Rev. B*, 1994, **50**, 17953.
30 G. Kresse, D. Joubert, *Phys. Rev. B*, 1999, **59**, 1758-1775.
31 J.P. Perdew, Y. Wang, *Phys. Rev. B*, 1992, **45**, 13244.
32 Y. Jeanvoine, J.G. Ángyán, G. Kresse, J. Hafner, *J. Phys. Chem. B*, 1998, **102**, 5573-5580.
33 F. Goltl, J. Hafner, *J. Chem. Phys.*, 2012, **136**, 064501-064517.
34 S.J. Clark, M.D. Segall, C.J. Pickard, P.J. Hasnip, M.J. Probert, K. Refson, M.C. Payne, *Z. Kristallogr.*, 2005, **220**, 567-570.
35 J.P. Perdew, K. Burke, M. Ernzerhof, *Physical Review Letters*, 1996, **77**, 3865.
36 S.-P. Gao, C.J. Pickard, M.C. Payne, J. Zhu, J. Yuan, *Physical Review B*, 2008, **77**, 115122.
37 V. Milman, K. Refson, S.J. Clark, C.J. Pickard, J.R. Yates, S.P. Gao, P.J. Hasnip, M.I.J. Probert, A. Perlov, M.D. Segall, *J. Mol. Struct.: THEOCHEM*, 2010, **954**, 22-35.
38 O. Sipr, *J. Synchrotron Rad.*, 2001, **8**, 232-234.
39 S.-D. Mo, W.Y. Ching, *Appl. Phys. Lett.*, 2001, **78**, 3809-3811.
40 F. Giordanino, P.N.R. Vennestrom, L.F. Lundegaard, F.N. Stappen, S. Mossin, P. Beato, S. Bordiga, C. Lamberti, *Dalton Trans.*, 2013, **42**, 12741-12761.
41 B. Hammer, J.K. Nørskov, Theoretical surface science and catalysis—calculations and concepts, in: H.K. Bruce C. Gates (Ed.) Advances in Catalysis, Academic Press, 2000, pp. 71-129.
42 W.F. Schneider, K.C. Hass, R. Ramprasad, J.B. Adams, *J. Phys. Chem. B*, 1998, **102**, 3692-3705.
43 I. Lezcano-Gonzalez, U. Deka, B. Arstad, A. Van Yperen-De Deyne, K. Hemelsoet, M. Waroquier, V. Van Speybroeck, B.M. Weckhuysen, A.M. Beale, *Phys. Chem. Chem. Phys.*, 2014, **16**, 1639-1650.

16 | *Catal. Sci. Technol.*, 2015, **00**, 1-15

This journal is © The Royal Society of Chemistry 20xx

44 M. Sano, S. Komorita, H. Yamatera, *Inorg. Chem.*, 1992, **31**, 459-463

45 E. Borfecchia, K.A. Lomachenko, F. Giordanino, H. Falsig, P. Beato, A.V. Soldatov, S. Bordiga, C. Lamberti, *Chem. Sci.*, 2015, **6**, 548-563.

46 T. Gunter, H.W.P. Carvalho, D.E. Doronkin, T. Sheppard, P. Glatzel, A.J. Atkins, J. Rudolph, C.R. Jacob, M. Casapu, J.-D. Grunwaldt, *Chem. Commun.*, 2015, **51**, 9227-9230.

47 F. Giordanino, E. Borfecchia, K.A. Lomachenko, A. Lazzarini, G. Agostini, E. Gallo, A.V. Soldatov, P. Beato, S. Bordiga, C. Lamberti, *J. Phys. Chem. Lett.*, 2014, **5**, 1552-1559.

48 L.S. Kau, D.J. Spira-Solomon, J.E. Penner-Hahn, K.O. Hodgson, E.I. Solomon, *J. Am. Chem. Soc.*, 1987, **109**, 6433-6442

49 G. Lamble, A. Moen, D.G. Nicholson, *J. Chem. Soc. Faraday Trans.*, 1994, **90**, 2211-2213

50 R. Zibaseresht, R.M. Hartshorn, *Acta Cryst.*, 2006, **E62**, i19-i22

51 B. Morosin, *Acta Cryst.*, 1976, **B32**, 1237-1240

52 T. Mizoguchi, I. Tanaka, S.-P. Gao, C.J. Pickard, *J. Phys. Conden. Matter*, 2009, **21**, 104204.

53 J.A. Bearden, A.F. Burr, *Rev. Mod. Phys.*, 1967, **39**, 125-142.

54 S.A. Guda, A.A. Guda, M.A. Soldatov, K.A. Lomachenko, A.L. Bugaev, C. Lamberti, W. Gawelda, C. Bressler, G. Smolentsev, A.V. Soldatov, Y. Joly, *J. Chem. Theory Comput.*, 2015, **11**, 4512-4521

This journal is © The Royal Society of Chemistry 20xx

Catal. Sci. Technol., 2015, **00**, 1-15 | **17**

263x122mm (150 x 150 DPI)